



저작자표시-비영리-변경금지 2.0 대한민국

이용자는 아래의 조건을 따르는 경우에 한하여 자유롭게

- 이 저작물을 복제, 배포, 전송, 전시, 공연 및 방송할 수 있습니다.

다음과 같은 조건을 따라야 합니다:



저작자표시. 귀하는 원저작자를 표시하여야 합니다.



비영리. 귀하는 이 저작물을 영리 목적으로 이용할 수 없습니다.



변경금지. 귀하는 이 저작물을 개작, 변형 또는 가공할 수 없습니다.

- 귀하는, 이 저작물의 재이용이나 배포의 경우, 이 저작물에 적용된 이용허락조건을 명확하게 나타내어야 합니다.
- 저작권자로부터 별도의 허가를 받으면 이러한 조건들은 적용되지 않습니다.

저작권법에 따른 이용자의 권리는 위의 내용에 의하여 영향을 받지 않습니다.

이것은 [이용허락규약\(Legal Code\)](#)을 이해하기 쉽게 요약한 것입니다.

[Disclaimer](#)

Alleviation of doxorubicin-induced
cardiotoxicity via
inhibition of TBL1X cleavage

Sun-Ho Lee

Department of Medical Science
The Graduate School, Yonsei University

Alleviation of doxorubicin-induced
cardiotoxicity via
inhibition of TBL1X cleavage

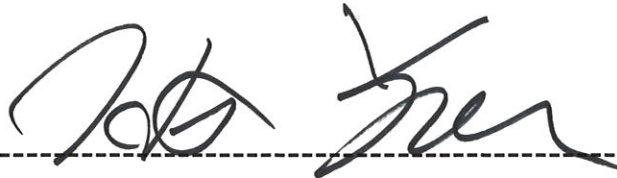
Directed by Professor Ho-Geun Yoon

The Doctoral Dissertation
submitted to the Department of Medical Science,
the Graduate School of Yonsei University
in partial fulfillment of the requirements for the degree of
Doctor of Philosophy of Medical Science

Sun-Ho Lee

December 2023

This certifies that the Doctoral Dissertation
of Sun-Ho Lee is approved.



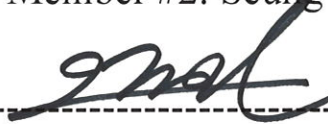
Thesis Supervisor: Ho-Geun Yoon



Thesis Committee Member #1: Sahng Wook Park



Thesis Committee Member #2: Seung-Hyun Lee



Thesis Committee Member #3: Jaewon Oh



Thesis Committee Member #4: Seok-Jun Kim

The Graduate School
Yonsei University

December 2023

<TABLE OF CONTENTS>

ABSTRACT	vii
I. INTRODUCTION	1
II. MATERIALS AND METHODS	5
1. Study samples	5
2. Immunohistochemistry (IHC), interpretation, and scoring	6
3. Cell culture and cardiomyocyte differentiation	6
4. Plasmid construction, siRNA, and transfection	7
5. Treatment of cells with caspase inhibitors	11
6. Western blotting and immunoprecipitation (IP)	11
7. <i>In vitro</i> translation and caspase cleavage assays	14
8. Duolink <i>in situ</i> proximity ligation assay (PLA).....	14
9. Analysis of apoptosis by flow cytometry and TUNEL assay	15
10. RNA isolation and quantitative RT-PCR.....	16
11. Immunocytochemistry (ICC)	16
12. Separation of cytoplasmic and nuclear extracts	17
13. Chromatin immunoprecipitation (ChIP) assay	17
14. TOP/FOP luciferase reporter assay	18
15. Adenovirus (AV) and Adeno-associated virus (AAV)	18
16. Multielectrode array (MEA) recording and analysis	19
17. Calcium transient assay	20
18. Animal experiment	20
19. <i>In vivo</i> cardiotoxicity model	21
20. Mouse echocardiography	21
21. Hematoxylin and eosin, and Masson's trichrome staining	22
22. Statistical analysis	23

III. RESULTS	24
1. The level of TBL1X is low in hearts of DCM patients	24
2. DOX-induced cleavage of TBL1X at D125, D136, and D215	28
3. Increased proteasomal degradation of TBL1X induced by caspase-3 activation in response to DOX	34
4. DOX-induced TBL1X cleavage increases apoptotic cell death in H9c2 cells	41
5. DOX-induced TBL1X cleavage blocks the Wnt/ β -catenin signaling pathway in H9c2 cells	45
6. DOX-induced TBL1X cleavage disrupts spontaneous electrophysiological responses in hiPSC-CMs	54
7. DOX-induced TBL1X cleavage disrupts calcium homeostasis in hiPSC-CMs	61
8. Inhibiting TBL1X cleavage improves cardiac function and ameliorates cardiac fibrosis in mice	63
IV. DISCUSSION	69
V. CONCLUSION	76
REFERENCES	77
ABSTRACT(IN KOREAN)	86
PUBLICATION LIST	89

LIST OF FIGURES

Figure 1. Low expression of TBL1X in cardiac tissues from patients with dilated cardiomyopathy (DCM)	26
Figure 2. Computational prediction of cleavage sites in the conserved sequence of TBL1X	30
Figure 3. Schematic representation of the expected cleaved forms of TBL1X	31
Figure 4. Cleavage of TBL1X at D125, D136, and D215 in H9c2 cells after DOX treatment	32
Figure 5. Identification of TBL1X cleavage dependent on caspase-3 and -7 through <i>in vitro</i> caspase assays	36
Figure 6. Cleavage and proteasomal degradation of TBL1X induced by caspase-3 activation through DOX	37
Figure 7. DOX-activated calpain has no effect on TBL1X cleavage ...	39
Figure 8. Destabilization of TBL1X via ubiquitin-dependent degradation after DOX treatment in H9c2 cells	40
Figure 9. Increased DOX-induced apoptosis in H9c2 cells with TBL1X depletion	42
Figure 10. Inhibition of TBL1X cleavage can mitigate the increase in DOX-induced apoptosis	43
Figure 11. Activation of the Wnt/ β -catenin signaling pathway inhibits DOX-induced apoptosis	47
Figure 12. Inhibition of TBL1X cleavage can alleviate the decrease in	

DOX-induced reduction of the Wnt/ β -catenin signaling pathway	48
Figure 13. DOX-induced TBL1X cleavage mediates its abnormal subcellular localization and induces nuclear translocation of β -catenin	50
Figure 14. Enhanced occupancy of WNT target gene promoters by TBL1X ^{uclv} compared to TBL1X ^{WT} under DOX treatment ..	52
Figure 15. Effects of TBL1X constructs on WNT activity in H9c2 cells under LiCl treatment.....	53
Figure 16. Validation of human induced pluripotent stem cells (hiPSCs) and hiPSC-derived cardiomyocytes (hiPSC-CMs)	56
Figure 17. Inhibition of TBL2X cleavage attenuates DOX-induced apoptosis in hiPSC-CMs	58
Figure 18. Reduced abnormal electrophysiological phenotypes induced by DOX in hiPSC-CMs treated with TBL1X ^{uclv}	59
Figure 19. Attenuation of abnormal Ca ²⁺ flux induced by DOX in hiPSCs treated with TBL1X ^{uclv} compared to TBL1X ^{WT}	62
Figure 20. Enhanced cardiac function in a DOX-induced cardiotoxicity mouse model treated with TBL1X ^{uclv}	64
Figure 21. Reduction in inflammation and apoptosis in a mouse model of DOX-induced cardiotoxicity treated with TBL1X ^{uclv}	66
Figure 22. Alleviation of DOX-induced cardiotoxicity via inhibition of TBL1X cleavage.....	68

LIST OF TABLES

Table 1. The primers used for cloning, qRT-PCR and ChIP assays	8
Table 2. The siRNA sequences	10
Table 3. The antibodies	12

ABSTRACT

Alleviation of doxorubicin-induced cardiotoxicity via inhibition of TBL1X cleavage

Sun-Ho Lee

*Department of Medical Science
The Graduate School, Yonsei University*

(Directed by Professor Ho-Geun Yoon)

Doxorubicin (DOX) is a widely used anthracycline anticancer agent. However, its irreversible effects on the heart can result in DOX-induced cardiotoxicity (DICT) post-cancer treatment. The pathophysiology of DICT has not yet been fully elucidated, and there are no effective strategies for its prevention or treatment. This study explores the novel role of Transducin beta-like 1X-linked (TBL1X) in both the development and regulation of DICT. TBL1X exhibits high expression in the normal heart, and its roles in nuclear factor kappa-light-chain-enhancer of activated B cells (NF- κ B) signaling pathway, subunit in co-repressor complex, and Wnt/ β -catenin signaling pathway have been elucidated.

In this study, a low expression of the TBL1X protein was observed in patients with

dilated cardiomyopathy (DCM). Moreover, these findings were attributed to the cleavage of TBL1X. In H9c2 cells, DOX treatment activated caspase-3 and -7, leading to significant cleavage of TBL1X. Inhibiting these caspases reduced TBL1X cleavage. Bioinformatics prediction analysis targeted Aspartate (D) residues at positions 125, 136, and 215, identified as sites for DOX-activated caspase-3-mediated cleavage.

To identify the cleavage sites, Aspartate (D) residues were substituted with Alanine (A) using site-directed mutagenesis, resulting in the generation of un-cleavable TBL1X (TBL1X^{uclv}) where all three sites were replaced. Unlike the TBL1X^{uclv}, the cleaved form of wild-type TBL1X (TBL1X^{WT}), through ubiquitin-dependent degradation, became destabilized, leading to reduced binding with β -catenin. Consequently, it failed to occupy the promoter regions of *Axin2* and *Ccnd1* genes, resulting in decreased activation of the WNT signaling pathway. Furthermore, the cell apoptotic signaling induced by DOX was also attenuated upon overexpressing of TBL1X^{uclv}.

To ascertain if the same outcomes were observed in both human cardiac cells and animal models, additional investigations were conducted. The results revealed that overexpression of TBL1X^{uclv} in normal human induced pluripotent stem cell-derived cardiomyocytes (hiPSC-CMs) mitigated cellular apoptosis and improved the cardiac functions, including diminished cardiac rhythmic function, delayed conduction, irregularities and abnormal calcium homeostasis induced by DOX. Also, utilizing adeno-associated virus (AAV) for cardiac-specific overexpression of TBL1X^{uclv} in mouse heart also ameliorated DOX-induced cardiomyocyte contractile dysfunction and collagen accumulation, thereby

reducing cardiotoxicity compared to the control group (TBL1X^{WT}).

In conclusion, these findings collectively demonstrate that caspase-3-mediated DOX-dependent cleavage of TBL1X inhibits Wnt/ β -catenin signaling, leading to cardiomyocyte apoptosis. Moreover, the novel role of TBL1X protein has been elucidated, providing insight into alleviating DICT during cancer treatment, thereby facilitating the development of effective therapeutic strategies.

Key words : transducin beta-like protein 1 X-linked, human induced pluripotent stem cell-derived cardiomyocytes, cardiomyotoxicity, doxorubicin, multi-electrode array

**Alleviation of doxorubicin-induced cardiotoxicity
via inhibition of TBL1X cleavage**

Sun-Ho Lee

*Department of Medical Science
The Graduate School, Yonsei University*

(Directed by Professor Ho-Geun Yoon)

I. INTRODUCTION

Doxorubicin (DOX) is an anthracycline chemotherapeutic agent discovered approximately half a century ago. It is widely employed in treating a diverse range of malignancies in both adults and children, attributable to its significant efficacy¹. Medications like DOX are subject to a maximum cumulative dose per patient. The dose is limited to reduce the risk of toxic side effects, such as cardiotoxicity. The incidence of DOX-induced cardiotoxicity is approximately 3%–5% at 400 mg/m² and up to 48% at > 700 mg/m² ^{2,3}. After its onset, DOX-induced cardiotoxicity causes arrhythmias with ventricular de-repolarization disturbances and decreases in left ventricular function, leading to dilated cardiomyopathy (DCM) and congestive heart failure^{4,5}. DOX-induced

cardiotoxicity (DICT) has also been shown to occur acutely and chronically⁶. Observations have indicated that arrhythmia, pathologic remodeling, dilation of all heart chambers, fibrosis, and heart failure are prevalent phenomena, as evidenced in previous studies^{7,8}. The mortality rate after a heart failure diagnosis is approximately 50% over a five year follow-up period⁹. DICT is consequently of global interest owing to the increasing number of cancer survivors who have received DOX treatment. While DICT is closely associated with a fatal prognosis, we currently lack suitable biomarkers to enable early detection or the development of effective treatment strategies¹⁰. The canonical mechanisms of DICT involve off-target inhibition of the cardiac DNA topoisomerase isoform 2B, mitochondrial accumulation, DNA and reactive oxygen species damage, culminating in cardiomyocyte injury or death^{7,9}. In rat cardiomyocytes H9c2 cells, mitochondrial damage was observed to disrupt calcium flux, thereby exacerbating DOX toxicity¹¹. Furthermore, the molecular mechanisms underlying DICT still need to be elucidated.

Transducin beta-like 1 X-linked (TBL1X), which contains F-box and WD-40 domains, was initially identified as part of the nuclear receptor co-repressor (NCoR)/silencing mediator for the retinoid and thyroid hormone receptor (SMRT) co-repressor complex, along with histone deacetylase 3 (HDAC3)^{20,21}. Subsequently, TBL1X, as an E3 ubiquitin ligase adaptor, degrades co-repressor complexes through the recruitment of specific ubiquitin/proteasome machinery, leading to the exchange of NCoR/SMRT co-repressors for co-activators upon ligand binding²². Recent studies elucidating the relationship between TBL1X and Wnt/ β -catenin signaling have demonstrated that TBL1X and β -catenin

mutually recruit each other to the promoter regions of *c-MYC* and *AXIN2*, Wnt target genes, and facilitate transcriptional activation and tumorigenesis²³. In addition, the sumoylation of TBL1X uncoupled from the NCoR co-repressor complex and conversely interacted with β -catenin, ultimately leading to the activation of Wnt target genes²⁴. In response to agents that cause DNA damage, p53-dependent Siah stabilization contributes to the formation of complexes comprised of Siah-interacting protein (SIP), Skp1, and TBL1X, affecting the activity of the β -catenin-Tcf/LEF transcription factor²⁵. More recently, it was discovered that TBL1X is essential for suppressing cardiomyocyte hypertrophy, as it facilitates the interaction between HDAC3 and GATA4²⁶. However, it remains unclear how TBL1X regulates heart function and Wnt/ β -catenin signaling.

The Wnt/ β -catenin signaling pathway is important for many aspects of development and homeostasis, including cell proliferation and migration, apoptosis, and genetic stability¹². This pathway is especially important, however, as it has protective effects against chemotherapeutic agents such as DOX in cardiomyocytes and cancer. In an animal model, Wnt inhibitors such as Dickkopf WNT signaling pathway inhibitor 1 (Dkk1) and protein kinase C gamma (PKC- ζ) exacerbate DICT^{13,14}. These studies show that adult cardiomyocytes, normal cells, are also subject to the DOX avoidance strategy used in cancer. Recent studies, in particular, have shown that DCM with the Lamin A/C (LMNA) mutation and arrhythmogenic right ventricular cardiomyopathy (ARVC) with the Plakophilin2 (PKP2)/Desmoplakin (DSP)/Desmoglein (DSG) mutation in animal models were responsible for suppressing Wnt signaling¹⁵⁻¹⁸. Given that genetic cardiomyopathy is

directly related to the incidence of DICT¹⁹, it is believed that the Wnt signaling regulator could be an important regulatory factor. These discrepancies further reveal the diversity in heart disease pathogenesis. Overall, the data indicate that Wnt/ β -catenin signaling is important in disease pathogenesis and that it appears to broaden the cellular spectrum of DICT.

To address this gap in knowledge, a novel function of the TBL1X protein is suggested as a regulator of Wnt/ β -catenin signaling in DICT. Specifically, the N-terminus cleavage of TBL1X by active caspase-3 is crucial for apoptosis induction via inhibition of Wnt/ β -catenin signaling in cardiomyocytes, and cleavage and apoptosis are effectively alleviated by the uncleaved mutant form of TBL1X (TBL1X^{uclv}). These findings were also validated in human induced pluripotent stem cell-derived cardiomyocytes (hiPSC-CMs) and *in vivo* DICT mouse models. These results suggest that TBL1X could serve as a novel therapeutic target for mitigating DICT, potentially paving the way for new clinical applications of DOX.

II. MATERIALS AND METHODS

1. Study samples

For experimental purposes, left ventricular (LV) samples were obtained from the explanted hearts of patients diagnosed with dilated cardiomyopathy (DCM) and undergoing cardiac transplantation. Clinical history, hemodynamic analysis, electrocardiogram, and Doppler echocardiogram data were systematically collected for each patient. Patients exhibiting LV systolic failure (ejection fraction, $EF \leq 40\%$) and a dilated, non-hypertrophic left ventricle (left ventricular dimension in end-diastole (LVDD) > 55 mm) using echocardiography were identified as having non-ischemic DCM ($n = 6$). Additionally, neither primary valvular nor ischemic heart diseases were present in the selected individuals. According to the functional classification established by the New York Heart Association, all patients were receiving medical care in accordance with the standards of the European Society of Cardiology. Transmural apex samples of the left ventricle were collected and preserved at -80 °C for subsequent RNA and protein extractions. Ethical approval for this study was granted by the Institutional Review Board (IRB) and ethics committee of the Yonsei University Health System (No. 4-2022-0853).

For immunohistochemistry (IHC), heart tissues from non-diseased donors served as control samples (Cat. No. HEN241a, US Biomax, Derwood, MD, USA, $n = 5$). The tissue microarray, comprising twenty-four samples from normal cardiac muscle tissues, was prepared using formalin-fixed and paraffin-embedded techniques. IHC analysis involved staining the tissues with antibodies specific to TBL1X.

2. Immunohistochemistry (IHC), interpretation, and scoring

For IHC, cardiac tissues from six patients who succumbed to DCM were utilized. Tissues were fixed in 4% formalin, paraffin-embedded, and sectioned into 4–5 μm thickness. IHC was performed using a Klear Mouse HRP with a DAB kit (GBI Lab, Bothell, WA, USA), following the manufacturer's protocol. Antigen retrieval was achieved by heating slides in citrate buffer (pH 6.0) for 30 min and were then treated with Protein Block Serum-Free blocking solution (Dako, Carpinteria, CA, USA) to reduce non-specific background staining. The primary antibody, anti-TBL1X, was incubated with the sections overnight at 4 °C. Visualization was achieved using 3,3'-diaminobenzidine (DAB), and the intensities of DAB staining were quantified with the IHC profiler plugin in ImageJ software.

3. Cell culture and cardiomyocyte differentiation

The H9c2 rat cardiomyocyte cell line, obtained from American Type Culture Collection (ATCC, Manassas, USA), was cultured in Dulbecco's modified Eagle medium (DMEM; Gibco, Carlsbad, CA, USA). The culture medium was supplemented with 10% fetal bovine serum (FBS; Gibco) and 1% antibiotic-antimycotic solution (Gibco). Cells were incubated in a humidified atmosphere with 5% CO_2 at 37 °C. Human induced pluripotent stem cells (hiPSCs) were cultured in TeSR-E8 medium (STEMCELL Technologies, Vancouver, BC, Canada) on vitronectin-coated plates. Cells were passaged every four days using ReLeSR reagent (STEMCELL Technologies). Cells were differentiated into cardiomyocytes according to a previously established protocol. For cardiomyocyte differentiation, cells

were seeded on Matrigel-coated six-well plates. At approximately 90% confluence, cells were incubated in Roswell Park Memorial Institute medium (RPMI) 1640+B27 supplement medium (Gibco) without insulin, supplemented with 10 μ M CHIR99021 (Tocris, Minneapolis, MN, USA) to activate Wnt signaling and induce mesoderm differentiation. After three days, the media was changed to RPMI1640 supplemented with B27, excluding insulin, alongside the addition of C59 (Selleckchem, Huston, TX, USA). After 48 hours, the medium was replaced with RPMI1640 supplemented with B27, containing insulin. Metabolic purification of the cardiomyocytes was achieved through glucose deprivation, using RPMI without glucose and supplemented with B27 containing insulin.

4. Plasmid construction, siRNA, and transfection

Various truncated-TBL1X expression plasmids were generated through standard PCR and subsequently sub-cloned into the pSG5 plasmid. To generate the Flag and Myc double-tagged TBL1X constructs, the pSG5-Flag plasmid was modified. The primer sequences used for sub-cloning are listed in **Table 1**. Using the QuickChange site-directed mutagenesis kit (Stratagene, La Jolla, CA, USA), Flag-TBL1X^{D125A}-Myc, Flag-TBL1X^{D136A}-Myc, Flag-TBL1X^{D215A}-Myc, and Flag-TBL1X^{uclv}-Myc expression plasmids were derived from Flag-TBL1X^{WT}-Myc. Additionally, Flag-TBL1X fragments (1–125aa, 1–136aa, 1–215aa, 126–577aa, 137–577aa, and 216–577aa) were constructed in the pSG5 plasmid using standard PCR sub-cloning. All plasmids were verified by DNA sequencing. Short interfering RNAs (siRNAs) targeting caspase-3, caspase-7, and TBL1X were

designed. Cells were transfected with these siRNAs (200 nM, chemically synthesized by Genolution, Seoul, Korea) using Lipofectamine RNAiMAX reagent (Thermo Fisher Scientific, Waltham, MA, USA) in 60-mm dishes, following the manufacturer's instructions. The siRNA sequences used in this study are listed in **Table 2**.

Table 1. The primers used for cloning, qRT-PCR and ChIP assays

Name	Sequence (5' to 3')
Site-directed mutagenesis primer sequence	
TBL1X^{D125A}	F: GGCACAGTGTTTCGCCGGCCGCCCCATA R: TATGGGGCGGCCGGCGAACACTGTGCC
TBL1X^{D136A}	F: CTGTCACTGATAGCCGCCGTGATGCCC R: GGGCATCACGGCGGCTATCAGTGACAG
TBL1X^{D215A}	F: CCAATGGAAATAGCTGGAGAGGTTGAG R: CTCAACCTCTCCAGCTATTTCCATTGG
TBL1X^{1-125aa}	F: GGCACAGTGTTTCGACTAACTCGAGCGGCCG R: CGGCCGCTCGAGTTAGTCGAACACTGTGCC
TBL1X^{1-215aa}	F: CCAATGGAAATAGATTA ACTCGAGCGGCCG R: CGGCCGCTCGAGTTAATCTATTTCCATTGG
TBL1X^{1-136aa}	F: CTGTCACTGATAGACTAACTCGAGCGGCCG R: CGGCCGCTCGAGTTAGTCTATCAGTGACAG
TBL1X^{126-577aa}	F: ACCTCTAGAGAATTCGGCCGCCCCATAGAG R: CTCTATGGGGCGGCCGAATTCTCTAGAGGT
TBL1X^{137-577aa}	F: ACCTCTAGAGAATTCGCCGTGATGCCCCGAC R: GTCGGGCATCACGGCGAATTCTCTAGAGGT
TBL1X^{216-577aa}	F: ACCTCTAGAGAATTCGGAGAGGTTGAGATT R: AATCTCAACCTCTCCGAATTCTCTAGAGGT

qRT-PCR primer sequence

TBL1X (human)	F: ACTCTTGGCTACGGGTCATA R: TTCGGTTCATTTC AAGGCAA
Axin2 (rat)	F: TAGGCGGAATGAAGATGGGC R: GTCCGGAAGAGGTATGCACC
c-Myc (rat)	F: CCAGCAGCGACTCTGAAGAAG R: GATGACCCTGACTCGGACCTC
Gapdh (rat)	F: TGATCTACCCACGGCAAGTT R: TGATGGGTTTCCCGTTGATGA

ChIP primer sequence

Axin2	F: CTGGAGCCGGCTGCGCTTTGATAA R: CGGCCCCGAAATCCATCGCTCTGA
c-Myc	F: AAGATCCTCTCTCGCTAATCTCC R: AGAAGCCCTGCCCTTCTC

Abbreviations: qRT-PCR, quantitative real-time PCR; ChIP, chromatin immunoprecipitation; TBL1X, transducin beta like 1X-linked; D, aspartate; A, alanine; Gapdh, glyceraldehyde-3-phosphate dehydrogenase; F, forward; R, reverse; aa, amino acid.

Table 2. The siRNA sequences.

Name	Sequence (5' to 3')
siControl	F: CCUCGUGCCGUUCCAUCAGGUAGUU R: CUACCUGAUGGAACGGCACGAGGUU
siCasp3	F: GCCGACUUCCUGUAUGCUUAC R: GUAAGCAUACAGGAAGUCGGC
siCasp7	F: GAUCCUGACCAGGGUGAAC R: GUUCACCCUGGUCAGGAUC
siTBL1X	F: GUAGACAAGACAACAAUAAUU R: UUAUUGUUGUCUUGUCUACUU

Abbreviations: siRNA (si-), small interfering RNA; Casp3, caspase-3; Casp7, caspase-7; TBL1X, transducin beta like 1 X-linked; F, forward; R, reverse.

5. Treatment of cells with caspase inhibitors

The pan caspase inhibitor Z-VAD-FMK (FMK001) and caspase-3 inhibitor Z-DEVD-FMK (FMK004) were acquired from R&D systems (Minneapolis, MN, USA). Calpain inhibitor-III (MDL-28170, S7394) was purchased from Selleckchem (Houston, TX, USA). Z-VAD (50 μ M), Z-DEVD (50 μ M), and Calpain inhibitor-III (10 μ M) were prepared by pre-mixing with the culture medium at the indicated concentrations. Each of inhibitor was dissolved in dimethyl sulfoxide (DMSO). Inhibitors were administered to the culture medium one hour prior to the doxorubicin hydrochloride (DOX) treatment. The DOX was purchased from chemscene (CS-1239, Monmouth Junction, NJ, USA).

6. Western blotting and immunoprecipitation (IP)

Cells were lysed using Cell Lytic Buffer M (Sigma-Aldrich, Burlington, MO, USA), enhanced with protease inhibitor (Nachlai Inc, San Diego, CA, USA), a phosphatase inhibitor cocktail (Calbiochem, Darmstadt, Germany), and 0.1 mM PMSF (Sigma-Aldrich). The obtained total lysates were subsequently utilized for western blotting and immunoprecipitation (IP) assays. Detailed information regarding the antibodies, including their working dilutions used in this study, can be found in **Table 3**. Quantification of western blotting images was performed using ImageJ software. For image analysis, RGB color images from western blotting were converted to 8-bit grayscale for quantification. Quantification involved measuring the mean gray values and integrated densities for each object in the images, following the guide instructions provided by ImageJ.

Table 3. The antibodies.

Name	Supplier	Cat no.	Dilution
Western blotting, Immunoprecipitation, and Chromatin immunoprecipitation			
TBL1X (epitope: 119-148 aa)	Santa Cruz Biotechnology	365661	1:1000
TBL1X (epitope: 211-577 aa)	Santa Cruz Biotechnology	137083	1:1000
Flag	Sigma Aldrich	A8592	1:10000
Myc	Cell Signaling Technology	2278	1:1000
HA	Santa Cruz Biotechnology	7392	1:1000
β-Actin	Santa Cruz Biotechnology	47778	1:1000
clv.Casp-3	Cell Signaling Technology	9661	1:1000
clv.Casp-7	Cell Signaling Technology	8438	1:500
clv.PARP-1	Cell Signaling Technology	9542	1:1000
p53	Cell Signaling Technology	2524	1:1000
β-catenin	Cell Signaling Technology	8480	1:1000
HDAC1	Cell Signaling Technology	5356	1:1000
Tubulin	Cell Signaling Technology	3873	1:1000

Immunocytochemistry			
TBL1X	Santa Cruz Biotechnology	365661	1:100
Flag	Sigma Aldrich	F3165	1:100
Myc	Cell Signaling Technology	2278	1:1000
β-catenin	Cell Signaling Technology	8480	1:100
SSEA4	Thermo Fisher Scientific	46-8843-42	1:100
OCT4	Cell Signaling Technology	9656	1:300
TRA-1-60	Thermo Fisher Scientific	13-8863-82	1:100
SOX2	Thermo Fisher Scientific	53-9811-82	1:100
NKX2.5	Thermo Fisher Scientific	PA5-49431	1:100
Titin	Proteintech Group	27867-1-AP	1:100
α-actinin	Thermo Fisher Scientific	A7811	1:100
MLC2V	Proteintech Group	10906-1-AP	1:500

Abbreviations: TBL1X, transducin beta like 1 X-linked; n, N-terminus; c, C-terminus; HA, haemagglutinin; Casp3, caspase-3; Casp7, caspase-7; clv, cleavage; PARP1, poly(ADP-ribose) polymerase 1; p53, tumor protein P53; HDAC1, histone deacetylase 1; SSEA4, stage-specific embryonic antigen 4; OCT4, octamer-binding transcription factor 4; TRA-1-60, podocalyxin; Sox2, SRY-box transcription factor 2; NKX2.5, NK2 homeobox 5; MLC2v, myosin light chain 2, ventricular/cardiac muscle isoform; WB, Western blot assay; IP, immunoprecipitation; ChIP, chromatin immunoprecipitation; IF, immunofluorescence assay.

7. *In vitro* translation and caspase cleavage assays

The pSG5-TBL1X construct was transcribed and translated using the TNT-coupled reticulocyte lysate system (Promega, Madison, WI, USA) incorporating [³⁵S]-methionine (PerkinElmer, Waltham, MA, USA) for labeling. *In vitro* translated TBL1X (2.5 μl) was incubated in a reaction buffer (50 μl) containing 50 mM HEPES, 50 mM NaCl, 0.1% CHAPS, 10 mM EDTA, 5% glycerol, 10 mM dithiothreitol at pH 7.2, with 100 ng of various recombinant caspases (caspase-2, -3, -6, -7, -8, -9, or -10) for 16 hours at 37 °C. Reactions were resolved on a 6% SDS-PAGE and analyzed using autoradiography for detection. Human recombinant caspase-2, -6, and -9 were procured from Merk Millipore (Burlington, MA, USA), caspase-3, -8, and -7 were obtained from BD biosciences (Franklin Lakes, NJ, USA), and caspase-10 was acquired from R&D systems.

8. Duolink *in situ* proximity ligation assay (PLA)

In situ proximity ligation assay (PLA) was conducted following the manufacturer's instructions (DUO92101, Sigma-Aldrich). Cells fixed with 4% cold paraformaldehyde were washed with PBS and subsequently incubated for 15 min in PBS containing 0.3% Triton X-100, washed, and then blocked with blocking solution. Subsequently, cells were incubated overnight at 4 °C with primary antibodies (FLAG and MYC) and washed three times for 10 min each with buffer A (1×TBS/0.05% Tween-20) under gentle agitation. The secondary antibodies/proximity probes, diluted in the same antibody diluent as the primary antibodies, were applied to the cells for 90 min at 37 °C. To remove unbound proximity

probes, the samples were washed four times, each for 10 min, with buffer A at room temperature, employing gentle agitation. Sections were incubated with ligation solution for 60 min at 37 °C, then washed twice for 10 min each with buffer A at room temperature. The rolling circle amplification-hybridization mixture was subsequently added and incubated for 120 min at 37 °C. After mounting, samples were examined under a Zeiss LSM710 confocal microscope (Carl Zeiss, Oberkochen, Germany). For detailed information, including working dilutions of the antibodies used, is summarized in **Table 3**.

9. Analysis of apoptosis by flow cytometry and TUNEL assay

Forty-eight hours post-transfection, H9c2 cells were treated with 2 μ M DOX at 37 °C for 24 h. Cells were washed twice with PBS, resuspended in Annexin V-binding buffer (422201, BioLegend, San Diego, CA, USA), and subsequently stained with Annexin V-fluorescein isothiocyanate (FITC; 640906, BioLegend) and Zombie NIR fixable dye (423105, BioLegend). Staining was performed in the dark at a temperature range of 18–22 °C for 15 min. Subsequently, about one times ten to the fifth cells per sample were analyzed using an LSR II flow cytometer (BD biosciences), with data processed using FLOWJO v10.0.7 software (BD biosciences). For the detection of apoptosis in cells and mouse heart tissues, DNA fragmentation was assessed using a TUNEL assay (terminal deoxynucleotidyl transferase-mediated dUTP nick end labeling) with an *in situ* Cell Death Detection Kit, Fluorescein (Roche, Basel, Switzerland) according to the manufacturer's instructions. Cells were first fixed with 4% cold paraformaldehyde in PBS for 30 min,

followed by a PBS wash. They were then permeabilized using 0.1% Triton X-100 in 3% BSA for 30 min, and then washed twice with PBS. The cells were then labeled with a mixture of TdT enzyme and label solution (comprising nucleotide mixture and fluorescein-dUTP in reaction buffer) at 37 °C for 60 minutes in the dark. Following a final rinse with PBS, the cells were analyzed under a fluorescence microscope, using excitation wavelengths of 450–500 nm and detection wavelengths of 515–565 nm.

10. RNA isolation and quantitative RT-PCR

Total RNA was extracted from cells utilizing the Ribospin Total RNA purification kit (GeneAll Biotechnology, Korea). Reverse transcription was performed using PrimeScript Reverse Transcriptase (Takara, San Jose, CA, USA), in accordance with the the manufacturer's instructions. Gene amplification was conducted using a QuantStudio 3 Real-Time PCR system (Applied Biosystems, Waltham, MA, USA) and FastStart Universal SYBR Green Master mix (Roche). The primer sequences used in this study are listed in **Table 1**.

11. Immunocytochemistry (ICC)

H9c2 cells were fixed with 4% paraformaldehyde for 15 min, blocked using a solution containing 5% bovine serum albumin (BSA; 9048-46-8, LPS solution, Daejeon, South Korea) and 0.3% Triton X-100 (USB, 9002-93-1), and then incubated overnight at 4 °C with primary antibodies targeting Flag-tag, Myc-tag, and β -catenin. For secondary antibody

staining, Alexa Fluor 488 chicken anti-rabbit IgG (A21441, 1:500, Thermo Fisher Scientific) and Alexa Fluor 568 goat anti-mouse IgG (A11030, 1:500, Thermo Fisher Scientific) were applied for 3 h at room temperature. Cell nuclei were counterstained using DAPI (NucBlue Fixed Cell ReadyProbes Reagent; R37606, Thermo Fisher Scientific) for 1 min at room temperature. The stained slides were examined using a LSM710 confocal microscope (Carl Zeiss) operated with ZEN blue edition software. Detailed antibody information is provided in **Table 3**.

12. Separation of cytoplasmic and nuclear extracts

The NE-PER nuclear and cytoplasmic extraction reagents kits (Thermo Fisher Scientific) was used to isolate cytoplasmic and nuclear extracts from H9c2 cells, following the manufacturer's instructions. Cells were harvested using trypsin-EDTA and subsequently centrifuged at 500 g for 5 min. The cell pellets were washed by resuspension in PBS and resuspended in 100 μ l ice-cold CER I buffer, followed by fractionation as per the manufacturer's instructions. To confirm the efficacy of the separation, antibodies targeting HDAC1 (Histone Deacetylase 1; a nucleus control protein) and tubulin (a cytoplasmic control protein) were utilized. Relative levels of nuclear proteins were normalized against HDAC1, and cytoplasmic protein levels were normalized against tubulin. Details on the control antibodies are provided in **Table 3**.

13. Chromatin immunoprecipitation (ChIP) assay

Approximately two times ten to the eighth cells were plated in 100-mm dishes, subsequently treated with 2 μ M DOX and transfected with the specified constructs. Post-treatment, cells underwent a fixation step with 1% formaldehyde in PBS for 10 min, followed by three rinses with cold PBS. Cross-linking was quenched by adding 125 mM glycine for 5 min at 24–26 °C. Subsequent procedures were performed as per the instructions of the Pierce Agarose ChIP Kit (Thermo Fisher Scientific), using a β -catenin antibody. Notably, sodium dodecyl sulfate (SDS) was excluded from all buffer solutions. Details of the primers used for amplification are listed in **Table 1**.

14. TOP/FOP luciferase reporter assay

Cells were seeded in 60-mm dishes one day before transfection. Cells were co-transfected with 1 μ g of TOPFLASH reporter plasmids (Promega) and the appropriate TBL1X expression plasmid. For control purposes and to measure transfection efficiency, the FOPFLASH luciferase vector (Promega) was employed. TOPFLASH plasmid harbors three Tcf/Lef binding sites upstream of a promoter driving the firefly luciferase gene. FOPFLASH, serving as a control to nonspecific activation, contains mutated Tcf/Lef binding sites. To normalize transfection efficiency in reporter assays, 0.05 μ g of a Renilla reniformis luciferase reporter, under a constitutive promoter, was co-transfected as an internal control. Luciferase activity was measured according to the manufacturer's instructions.

15. Adenovirus (AV) and Adeno-associated virus (AAV)

To achieve stable overexpression of TBL1X variants in both iPSC-CMs and mouse hearts, TBL1X was amplified using standard PCR techniques. For iPSC-CMs, the amplified TBL1X was sub-cloned into the pEntCMV-EF1a-GFP shuttle vector, while for mouse hearts, it was sub-cloned into Virovek's AAV shuttle vector. Site-directed mutagenesis was employed to generate the TBL1X^{uclv} plasmid, using pEntCMV-TBL1X^{WT}-EF1a-GFP (Ad-TBL1X^{WT}) for iPSC-CMs and pFB-CMV-TBL1X^{WT}-T2A-GFP-WRE-bGHpA (AAV9-TBL1X^{WT}) as templates. The resulting plasmids, Ad-TBL1X^{uclv} for iPSC-CMs and AAV9-TBL1X^{uclv} for mouse hearts, were verified through DNA sequencing.

Virus production for both applications was outsourced to Koma Biotechnology (Seoul, Korea). For iPSC-CMs, viruses were propagated in a monolayer culture of HEK 293 cells, and for mouse hearts, Sf9 insect cells were cultured in Sf-900 II serum-free medium. In the case of HEK 293 cells, pronounced cytopathic effects led to the centrifugation of virus-containing media at 1500 rpm for 10 minutes. Conversely, Sf9 cells were triple-infected with baculovirus vectors coding for replication and structural proteins and AAV vector genomes to produce AAV9 and AAV-PHP.B vectors. These were harvested post 3-day infection and centrifuged at 3000 rpm for 15 minutes. Following centrifugation, the viruses for both applications underwent purification on sequential cesium chloride gradients. The purified viruses were then dialyzed for iPSC-CMs, dialysis was in PBS containing 10% glycerol (pH 7.4), while for mouse hearts, a PD-10 desalting column (GE HealthCare,

Piscataway, NJ, USA) was used.

For both applications, 10 μ L of the viral sample was added to 990 μ L of 0.1% SDS buffer and incubated between 18–22 °C for 15 minutes before measuring the optical density (OD) at A260. The titers for both AV and AAV were calculated using the formula: virus titer in viral particles (vp)/mL = OD value \times dilution factor \times one point one times ten to the twelfth.

16. Multielectrode array (MEA) recording and analysis

The iPSC-derived cardiomyocytes were seeded onto a 50 mg/mL fibronectin-coated CytoView MEA 24-well plate (Axion Biosystems, Zurich, Switzerland) at a density of 50,000 cells per well seven days prior to each assay. Activity was recorded before treatment (baseline), immediately after the DOX treatment (0 h), and 24 h post-treatment with DOX using the Maestro Edge MEA system (Axion Biosystems). DMSO served as the vehicle control, and an equal volume of either the vehicle control or DOX was added to the wells. Field potentials (FP) were analyzed using the platform software, and outputs included beat period (s), spike amplitude (mV), and field potential duration (FPD, ms). Raw FPD measurements were also corrected using Fredericia's rate correction algorithm (FPDcF), where $FPDc = FPD/Beat\ period^{0.33}$. All recordings were captured using the standard cardiac settings (v2.1.1.5) at 37 °C.

17. Calcium transient assay

iPSC-derived cardiomyocytes were seeded in matrigel-coated 35-mm glass bottom

dishes (MATTEK, P35G-1.5-20-C, Ashland, MA, USA). Cardiomyocytes were loaded with 5 μ M Rhod-2 AM fluorescent calcium indicator (R1244, Thermo Fisher Scientific) for 20 min and then recorded in Tyrode's solution (T2397, Sigma-Aldrich) in the temperature range of 18–22 °C. Spontaneous Ca^{2+} transients were acquired using a line scan mode. A total of 10,000 lines were acquired over a 61 s recording. For the Ca^{2+} transient recording, confocal line-scan imaging was performed on resting cells at 552 nm excitation and 581 nm emission using a Zeiss LSM710 inverted confocal microscope at 20 \times magnification. The Ca^{2+} transients were processed using ZEN software and analyzed using Microsoft Excel.

18. Animal experiment

C57BL/6Jms Slc mice (eight-week-old) were obtained from the Japan Sankyo Labo Service Corporation (Shizuoka, Japan). All animal experimental procedures in this study were approved by Yonsei University Health System Institutional Animal Care and Use Committee (IACUC No. 2018-0269, 2022-0033). Inhalation anesthetic was administered in an induction chamber with 5% isoflurane in 100% oxygen at a constant flow rate of 1.0 liters per minute (LPM) for 5 min. The animals were then ventilated using a VentElite small rodent ventilator (Harvard Apparatus, 55-7040) at 120 respirations per minute with a 2.4 ml stroke volume. Anesthesia was maintained with 2% isoflurane mixed with 100% oxygen throughout the surgery. Sterile lubricating eye ointment (prednilone) was applied following the induction of anesthesia to prevent corneal drying. Isoflurane ventilation was

reduced to zero after completion of the surgery. Once spontaneous breathing was evident, the endotracheal tube was removed. Subsequently, C57BL/6J mice were injected with either AAV9-TBL1X^{WT} or AAV9-TBL1X^{uclv} via single intramyocardial injections (i.c.). A dosage of one times ten to the ninth plaque-forming units per mouse was used for adeno-associated virus delivery. The mice used in the *in vivo* experiments were euthanized humanely using CO₂ gas. Heart tissue was harvested after mice were sacrificed, and tissues were fixed in 4% paraformaldehyde and then embedded in paraffin for serial sectioning.

19. *In vivo* cardiotoxicity model

For a 25 g mouse, DOX was administered by dissolving it fresh in 200 μ L of 0.9% saline solution to 0.125 mg/ml for each injection. To induce cardiotoxicity, the prepared 5 mg/kg DOX was administered intraperitoneally (i.p.) once a week for a duration of 4 weeks (cumulative dose 20 mg/kg), while saline was injected instead of DOX in the control group. Echocardiography was performed 7 days after the final DOX administration, and tissues were collected for experimentation. Also, we calculated Ejection fraction (EF%) and Fractional shortening (FS%) based on M-mode echocardiographic images by referring to previously studies²⁷.

20. Mouse echocardiography

Mice were anesthetized in a pre-filled induction chamber with 4% isoflurane in 1.0 L/min O₂ and then treated with a chemical hair remover to optimize the acoustic interface.

Then, echocardiographic examination was performed under the condition with 1% isoflurane in oxygen on the heating pad of the Vevo imaging system. Echocardiography was performed using a VisualSonics Vevo 2100 Imaging System (Toronto, Canada) coupled with a MicroScan Transducer (White MS 550) operating at 40 MHz. B-mode cine loops were generated to visualize the maximum dimension of the left ventricle (LV) from the apex to the base in a parasternal short axis view. M-mode echocardiographic images at the papillary muscle level were obtained from a short view to measure the size and function of the left ventricle. All acquired images were digitally stored in raw format (DICOM) for further offline-analysis. To calculate Ejection fraction (EF) and Fractional shortening (FS) parameters, formulas²⁷ were used as follows: $FS\% = [LVIDd - LVIDs] / LVIDd \times 100\%$, $EF\% = [(LVIDd)^3 - (LVIDs)^3] / [LVIDd]^3 \times 100\%$. During the mice echocardiography, ECG (Electrocardiogram) was simultaneously recorded.

21. Hematoxylin and eosin, and Masson's trichrome staining

The cardiac specimens were fixed using 4% buffered paraformaldehyde, embedded in paraffin, and cut into 4–5 μm -thick sections, which were stained with hematoxylin and eosin (H&E). Masson's trichrome staining (MTS) was performed using an MT kit (StatLab, American MasterTech, Lodi, CA, USA) according to the manufacturer's instructions. Briefly, the embedded sections were deparaffinized and rinsed with 100% ethanol and water, respectively. The slides were incubated with Bouin's fluid at 4 °C for 1 h. Subsequently, they were sequentially incubated with Weiger's working hematoxylin,

Biebrich scarlet acid fuchsin, phosphomolybdic/phosphotungstic acid, aniline blue stain, and 1% acetic acid. Finally, the slides were dehydrated and mounted. Fibrosis in the cardiac tissues was assessed using fluorescent microscopy (OLYMPUS, IX71, Tokyo, Japan).

22. Statistical analysis

To ensure data normality, the distribution of the data was assessed using the Shapiro-Wilk normality test. Based on the results, with $p\text{-value} \geq 0.05$, confirming the normality of the data, and data were analyzed using student's t-test or one-way analysis of variance (ANOVA) with Tukey's multiple comparison test. Values are expressed as the mean \pm SD. Statistical analyses were conducted using Prism 8 (GraphPad Software, La Jolla, CA, USA). Statistical significance was set at * $p < 0.05$, ** $p < 0.01$, *** $p < 0.005$, and **** $p < 0.0005$.

III. RESULTS

1. The level of TBL1X is low in hearts of DCM patients

This study aimed to ascertain if dilated cardiomyopathy (DCM) leads to changes in TBL1X protein levels, its expression was compared between cardiac tissues from DCM patients and normal individuals. Cardiac tissue samples were subjected to immunohistochemistry (IHC) using antibodies specific for TBL1X. IHC analysis revealed a significant reduction in TBL1X expression, approximately 75%, in cardiac tissues from DCM patients (Figure 1A). To check whether this reduction was due to a decrease in TBL1X transcription in DCM patients, microarray data from the Gene Expression Omnibus (GEO) were analyzed. Among the GEO datasets, the mRNA expression of TBL1X did not change between normal individuals and DCM patients (Figure 1B). Because the DOX-induced toxicity causes pathological features and phenotype in the heart that closely resembles DCM²⁸⁻³⁰, additional cardiac tissues from two patients who experienced DICT following DOX treatment was obtained. Both patients completed treatment sessions, receiving total cumulative dose of 300 mg/m² and 360 mg/m², respectively. Furthermore, they were diagnosed with DCMP following DOX administration and subsequently underwent recent heart transplantation. The possibility of TBL1X cleavage in patients with idiopathic and DICT-induced DCM was explored (Figure 1C). Interestingly, in heart tissues from the DICT patients with DCM, two bands suspected

to be cleaved-TBL1X were more clearly observed under the bands of full-length TBL1X. This phenomenon was more pronounced in the DICT patient group. Normal human induced pluripotent stem cell-derived cardiomyocytes (hiPSC-CMs) were used as a control. Taken together, these results indicate that the TBL1X expression level changes in the patients with DCM occurred at a post-translational level.

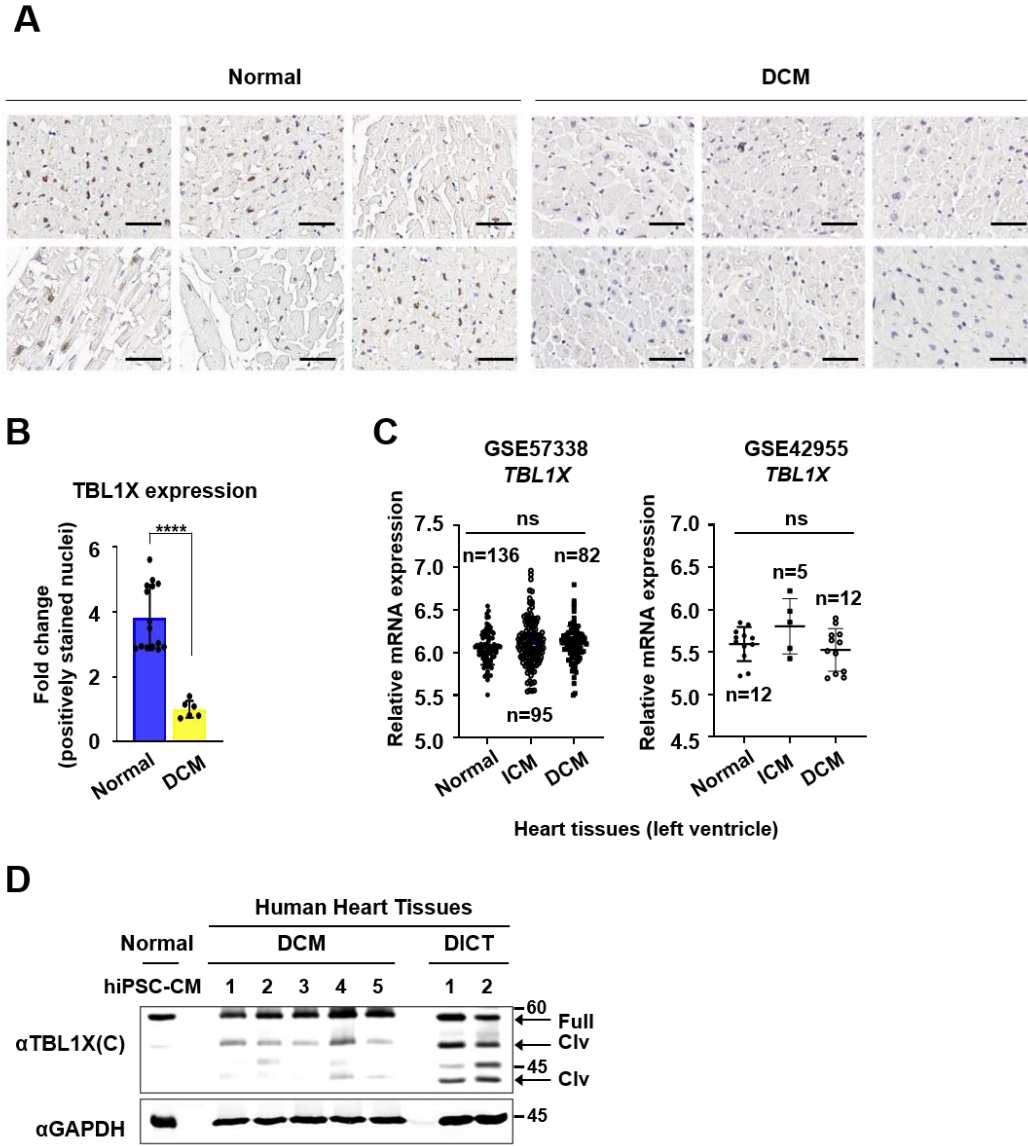


Figure 1. Low expression of TBL1X in cardiac tissues from patients with dilated cardiomyopathy (DCM). (A) TBL1X expression in cardiac tissues from patients with DCM (n = 6) compared to normal cardiac tissues (n = 15). TBL1X expression is low in the

cardiac tissues of patients with DCM. Slides were stained with an antibody against an N-terminal TBL1X epitope using immunohistochemistry (IHC). Representative images are shown. Scale bar = 50 μ m (left panel). (B) The DAB (3,3'-diaminobenzidine) staining intensity score was calculated using the IHC profiler plugin in ImageJ software (right panel). **** $p < 0.0001$ (Student's t -test) (C) Data from publicly available datasets on TBL1X expression levels in cardiac tissues from patients with DCM and normal cardiac tissues. GSE57338, $n = 313$ (normal $n = 136$, iCMP $n = 95$, iDCMP $n = 82$); GSE42955 $n = 29$ (normal $n = 5$, iCMP $n = 12$, DCMP $n = 12$). Quantification of TBL1X mRNA levels by microarray (two probes; ILMN_1248994 and ILMN_2624451) in the GSE57337 and by RNA sequencing in GSE42955. (D) TBL1X cleavage in heart tissues sampled from patients with idiopathic and DICT-induced DCM. Proteins were immunoblotted with the indicated antibodies. The arrows indicate cleaved-TBL1X. n.s., no significance. iCMP, ischemic cardiomyopathy; iDCMP, idiopathic dilated cardiomyopathy.

2. DOX-induced cleavage of TBL1X at D125, D136, and D215

Due to the high homology of TBL1X in both human and rat, to examine whether DOX induces TBL1X changes, TBL1X was identified after the DOX treatment in H9c2 cells, rat cardiomyocytes, using two antibodies against its N- or C-termini, respectively. Concordantly, a decrease in endogenous TBL1X expression was observed in both antibodies, but interestingly, the cleaved-TBL1X was detected only when using the C-termini antibody in a time-dependent manner after the DOX treatment (Figure 4A). The feasibility of using multiple cardiac cell lines was because of the significance conservation of human TBL1X and other inter-species protein homologies (mouse, 94.3%; rat, 94.3%).

Seven caspase-dependent candidate sites were identified in TBL1X that were found to be critical for DOX-mediated cleavage when using bioinformatics analysis (CaspDB2, <http://caspdb.sanfordburnham.org>) (Figure 2). To identify the specific cleavage sites, a TBL1X construct double tagged with Flag and Myc at its N- and C-termini was generated (Flag-TBL1X-Myc), and it replaced TBL1X Asp-125 (D125), Asp-136 (D136), or Asp-215 (D215) with Ala (A) through site-direct mutagenesis. An additional TBL1X mutant was generated in which all three sites were substituted with A (uncleaved mutant; uclv) (Figure 3). The sequences of TBL1X at positions D125, D136, and D215, are well-conserved in human, rat, and mouse. Each plasmid was overexpressed in H9c2 cells and then treated with DOX. Among the three cleaved-TBL1X bands, the 49 kD fragment disappeared at TBL1X^{D125A}, the 47.7 kD fragment at TBL1X^{D136A}, and the 40 kD fragment at TBL1X^{D215A}.

However, cleaved-TBL1X bands were not observed in TBL1X^{uc1v} (Figure 4B). To verify the importance of these three sites in TBL1X for its cleavage, a proximity ligation assay (PLA) was performed using a double Flag-TBL1X-Myc construct for the *in situ* visualization and quantification of TBL1X cleavage. DOX efficiently induced the cleavage of TBL1X^{WT}, which failed to produce rolling circle amplification (RCA). However, TBL1X^{uc1v} successfully formed RCA in DOX-exposed H9c2 cells (Figure 4C).

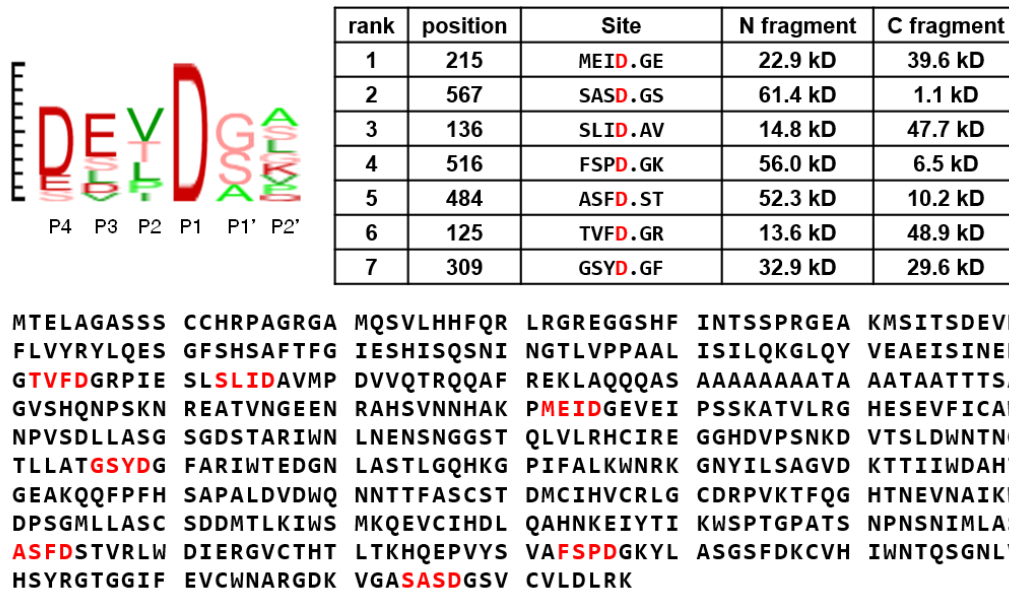


Figure 2. Computational prediction of cleavage sites in the conserved sequences of TBL1X. The cleavage probability of TBL1X was predicted using CaspDB2 (<http://caspdb.sanfordburnham.org>). P4-P2' indicates target sequences in TBL1X. Cleavage was predicted to occur between P1 and P1'. Specific information, including specificity for the seven predicted positions, is listed in the table (upper panel). The seven predicted cleavage target sequences are highlighted in red (lower panel). D; aspartate. N: N-terminus. C; C-terminus.

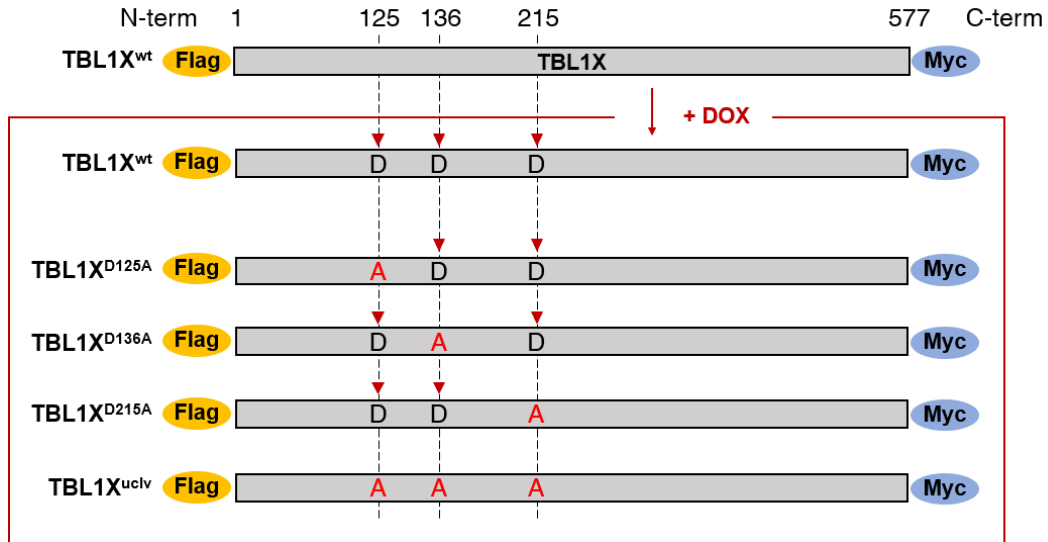


Figure 3. Schematic representation of the expected cleaved forms of TBL1X. The diagrams show the possible cleavage of the Flag-TBL1X^{WT}-Myc plasmid construct. For the TBL1X^{D125A}, TBL1X^{D136A}, and TBL1X^{D215A} mutants, cleavage is expected at the remaining two positions except for the mutation site. Red inverted triangles indicate the cleavage sites by DOX. D; aspartate, A; alanine.

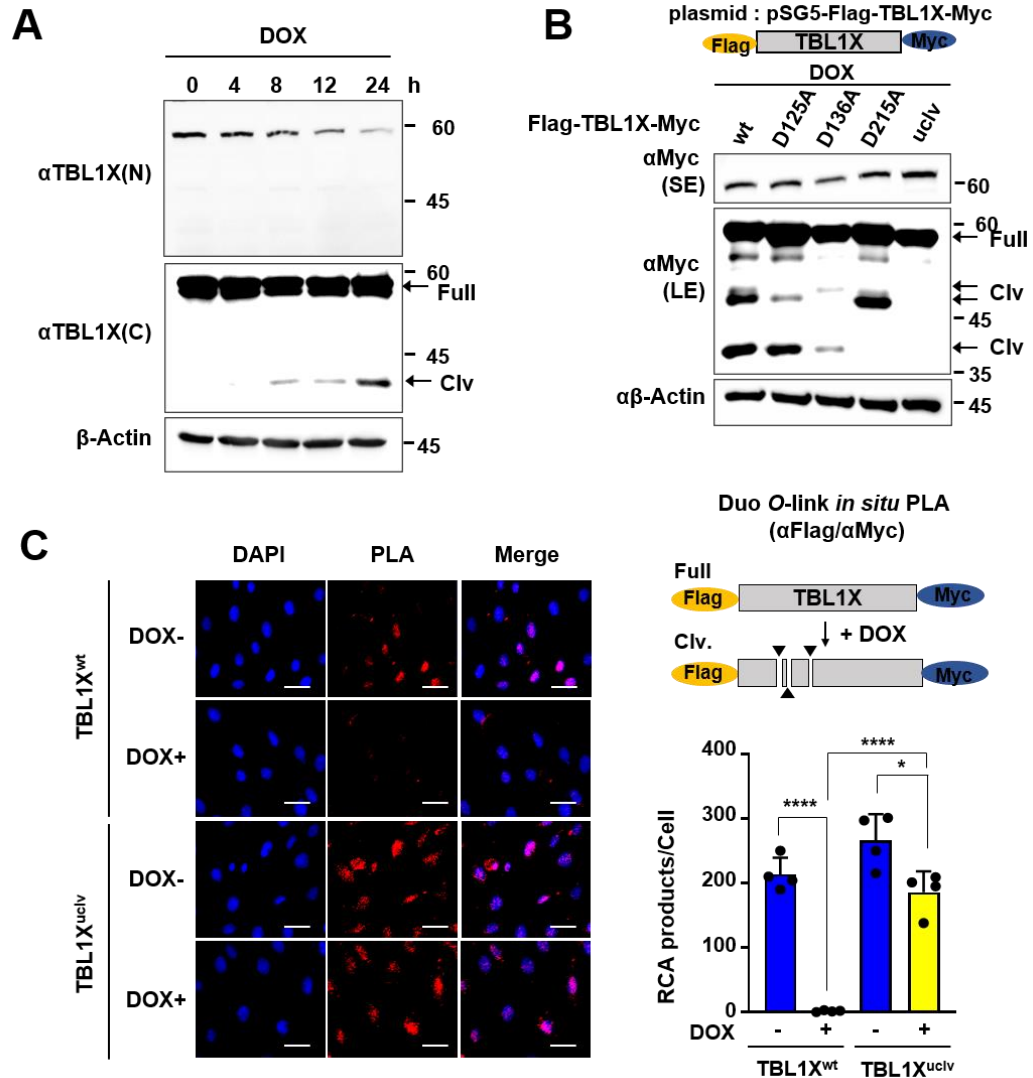


Figure 4. Cleavage of TBL1X at D125, D136, and D215 in H9c2 cells after DOX treatment. (A) Endogenous TBL1X was cleaved in a time-dependent manner following DOX treatment. H9c2 cells were treated with 2 μ M DOX, and total proteins were extracted and immunoblotted with the indicated antibodies. (B) TBL1X cleaved at D125, D136, and

D215 in response to DOX. Wild-type TBL1X (TBL1X^{WT}), TBL1X^{D125A}, TBL1X^{D136A}, TBL1X^{D215A}, or mutations at three sites (TBL1X^{clv}) were overexpressed in H9c2 cells which were then harvested and lysed to extract the protein. The total protein was used for immunoblot assays. Blue stars indicate cleaved TBL1X bands. (C) TBL1X^{clv} abrogates its cleavage in response to DOX. H9c2 cells were transiently transfected with a double-tagged TBL1X (Flag-TBL1X-Myc) plasmid and treated with DOX. Permeabilized cells were incubated with antibodies against Flag and Myc, and PLA probes added. The cell nuclei were counterstained with DAPI (blue). Red dots represent RCA products from immunoreactions detected using fluorescently-labeled complementary oligonucleotides. Representative images of four independent experiments are shown. Scale bar = 50 μ m (upper panel). The number of RCA products per cell from these images is shown in the bar graph. The values are presented as the mean \pm S.D. from three independent experiments (lower panel). * $p < 0.05$ and **** $p < 0.0001$ (Student's t -test). SE, short exposure; LE, long exposure. clv: cleaved protein. PLA; proximity ligation assay. RCA; rolling circle amplification.

3. Increased proteasomal degradation of TBL1X induced by caspase-3 activation in response to DOX

To investigate whether caspase is involved in the cleavage of TBL1X following DOX treatment, caspase assays were performed using an *in vitro* translation system (Figure 5A). Caspase-3 and -7 predominately caused TBL1X cleavage. To confirm this, a caspase-3/-7 specific inhibitor, Z-DEVD, was used to treat H9c2 cells. Concordantly, the DOX-induced TBL1X cleavage was abrogated following the Z-DEVD treatment in combination with DOX. The treatment with Z-VAD, a pan-caspase inhibitor, exhibited similar results (Figure 6A). There are other proteases that could potentially be involved in the cleavage of TBL1X, such as calpain, which has been reported to be activated by DOX. I examined whether calpain can trigger the cleavage of TBLX. Initially, through a computational prediction program (Procleave), it was identified three potential cleavage sites of TBL1X by calpain-1 and calpain-2, respectively (Figure 7A). Subsequently, the changes of TBL1X induced by DOX after treatment with CI-III (Figure 7B). A small interfering RNA (siRNAs) was used to assess if DOX-induced TBL1X cleavage had specificity to caspase-3 or -7. Notably, following the caspase-3 knockdown, DOX-induced TBL1X cleavage was considerably reduced (Figure 6B). Furthermore, in caspase-3 assays using *in vitro* translation systems, the expected cleaved bands were detected in TBL1X^{WT} and TBL1X mutants; however, cleavage was not observed in TBL1X^{uclv} (Figure 5B). These results collectively indicate that DOX induces TBL1X cleavage at D125, D136, and D215 in a caspase-3-dependent

manner.

DOX treatment triggers significant ubiquitination associated with a decline in protein translation³¹. Considering that DOX treatment leads to TBL1X cleavage and a reduction in its levels, further investigation was carried out to determine if the degradation was attributable to its decrease. For this purpose, TBL1X levels were analyzed after the DOX treatment with or without MG132, a proteasomal inhibitor. The results showed that 8 h after the DOX treatment, approximately 20% of the TBL1X was detected in its cleaved form in the presence of MG132. Then, 24 h after the DOX treatment, over 40% of the full-length TBL1X was cleaved (Figure 6C). To complement this, a ubiquitination assay was conducted on H9c2 cells. TBL1X was ubiquitinated following the DOX treatment in a time-dependent manner (Figure 8A). To confirm whether ubiquitination of TBL1X was associated with its cleavage, we overexpressed either TBL1X^{WT} or TBL1X^{uclv} and performed ubiquitination assays. DOX-induced ubiquitination of TBL1X^{WT} was substantially increased, whereas TBL1X^{uclv} was not ubiquitinated (Figure 8B). These results indicate that DOX-induced TBL1X cleavage leads to the ubiquitin-dependent degradation of TBL1X.

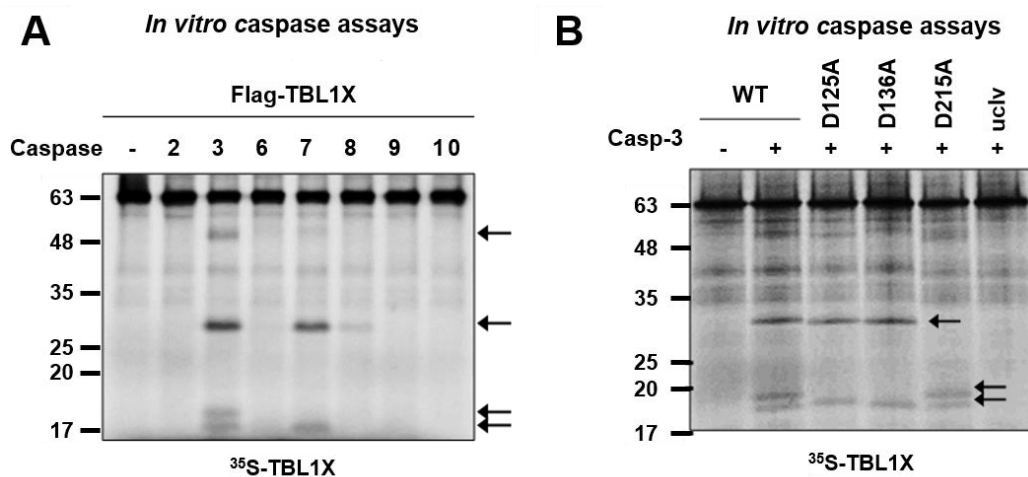


Figure 5. Identification of TBL1X cleavage dependent on caspase-3 and -7 through *in vitro* caspase assays. (A) TBL1X was labeled with ³⁵S-labeled methionine (³⁵S-Met) through *in vitro* translation and subsequently used as a substrate for caspase detection assays. ³⁵S-labeled TBL1X was detected by autoradiography. The arrows indicate cleaved TBL1X bands. (B) TBL1X^{uclv} mutant is not cleaved by caspase-3 in a cell-free system. TBL1X^{WT}, TBL1X^{D125A}, TBL1X^{D136A}, TBL1X^{D215A}, and TBL1X^{uclv} mutants were labeled with ³⁵S using *in vitro* translation and sequentially incubated with the recombinant caspase-3 enzyme. ³⁵S-labeled TBL1X was detected by autoradiography. The arrows indicate cleaved-TBL1X bands. D; aspartate. A: alanine.

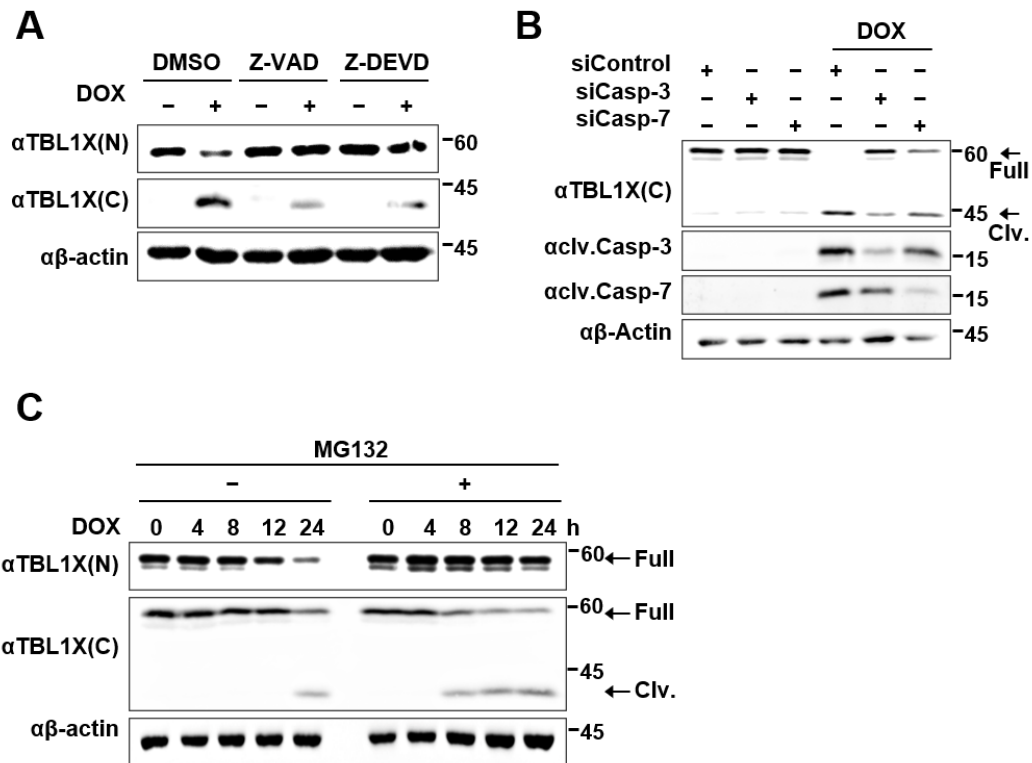


Figure 6. Cleavage and proteasomal degradation of TBL1X induced by caspase-3 activation through DOX. (A) TBL1X cleavage was blocked following the treatment of caspase inhibitors. H9c2 cells were exposed to either pan-caspase inhibitor (Z-VAD) or caspase 3/7 specific inhibitor (Z-DEVD) with or without 2 μ M DOX for 24 h. The cells were lysed, and protein extracts were used for immunoblot assays with the indicated antibodies. (B) In the DOX response, TBL1X is cleaved in a caspase-3-dependent manner. siCaspase-3 or siCaspase-7 was transiently transfected, and subsequently, H9c2 cells were treated with 2 μ M DOX for 24 h. Protein extracts from the cells were immunoblotted with the indicated antibodies. (C) MG132 treatment induces the accumulation of TBL1X

cleavage. Endogenous TBL1X was cleaved in a time-dependent manner following DOX treatment. The cells were treated with 1 μ M DOX for the indicated time and 10 μ M MG132 for 12 h. Cells were incubated for the indicated time, and whole-cell lysates were immunoblotted using the indicated antibodies. Arrows indicate cleaved TBL1X. N: N-terminus. C: C-terminus.

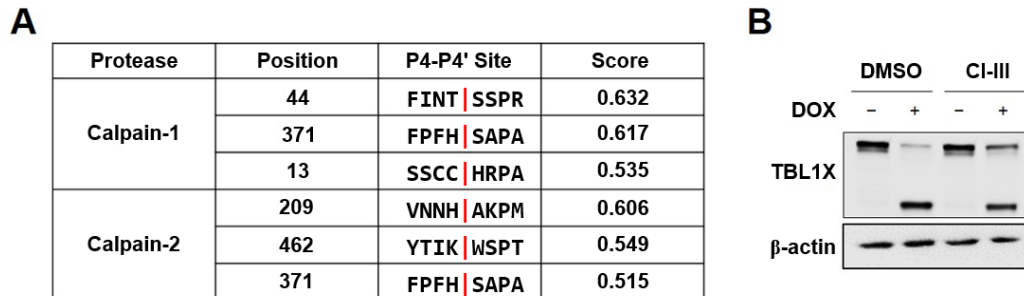


Figure 7. DOX-activated calpain has no effect on TBL1X cleavage. (A) The cleavage probability of TBL1X was predicted using Procleave biotools (procleave.erc.monash.edu/). P4-P4' indicates target sequences in TBL1X. Cleavage was predicted to occur between P1 and P1'. The seven predicted cleavage target sites are highlighted in red. (B) The DOX-induced TBL1X cleavage is independent of calpain. H9c2 cells were exposed 10 μ M of CI-III, a calpain-1 and -2 inhibitor, with or without 2 μ M of DOX for 24 h. The cells were lysed, and protein extract were used for immunoblot assays with the indicated antibodies. CI-III: calpain inhibitor III (MDL-28170). DMSO: dimethyl sulfoxide.

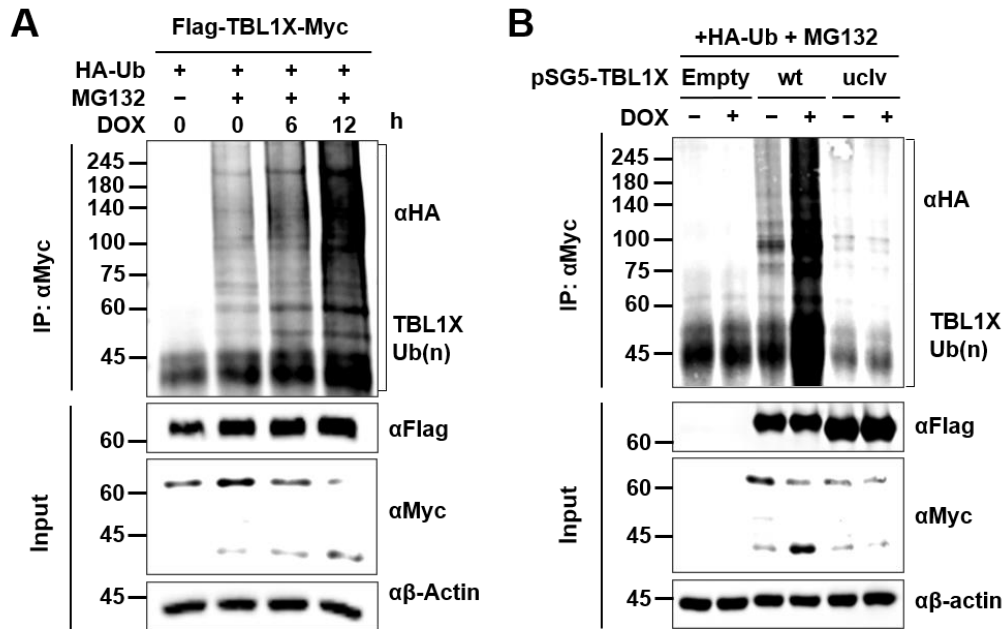


Figure 8. Destabilization of TBL1X via ubiquitin-dependent degradation after DOX treatment in H9c2 cells. (A) TBL1X ubiquitination increases in response to DOX in a time-dependent manner. H9c2 cells were transfected HA-tagged Ub plasmid and treated with 10 μ M MG132 with or without 1 μ M DOX for the indicated time. Whole-cell lysates were immunoprecipitated with an anti-TBL1X(C) antibody and immunoblotted with the indicated antibodies. (B) The TBL1X^{uclv} mutation abolishes DOX-induced TBL1X ubiquitination. H9c2 cells were transfected with HA-Ub and the indicated Myc-tagged TBL1X plasmids and then treated with 10 μ M MG132 with or without 1 μ M DOX for 24 h. Whole-cell lysates were immunoprecipitated with anti-Myc antibody and immunoblotted. Ub: ubiquitination.

4. DOX-induced TBL1X cleavage increases apoptotic cell death in H9c2 cells

To determine whether TBL1X is involved in DOX-induced apoptotic cell death in cardiomyocytes, the expression of the predominant factors mediating apoptotic cell death was investigated. Cleaved-PARP1, cleaved-caspase-3, and p53 were increased following DOX-induced TBL1X cleavage (Figure 9A). To confirm TBL1X involvement in this phenomenon, the TBL1X was depleted using siRNAs, and the pro-apoptotic factor levels were monitored. The expression of these factors was more highly upregulated in TBL1X knocked-down cells than in control cells (Figure 9B). Notably, TBL1X^{uclv}-overexpressing cardiomyocytes showed lower levels of apoptotic factors than in TBL1X^{WT}-overexpressing cells in response to the DOX treatment (Figure 10A). Consistently, TBL1X^{uclv} overexpression resulted in significantly less apoptotic cell death than TBL1X^{WT} overexpression in the presence of DOX (Figure 10B). This result was further confirmed by the TUNEL staining (Figure 10C). Collectively, these findings suggest that DOX-induced TBL1X cleavage increases the expression of pro-apoptotic factors, resulting in cardiomyocyte death.

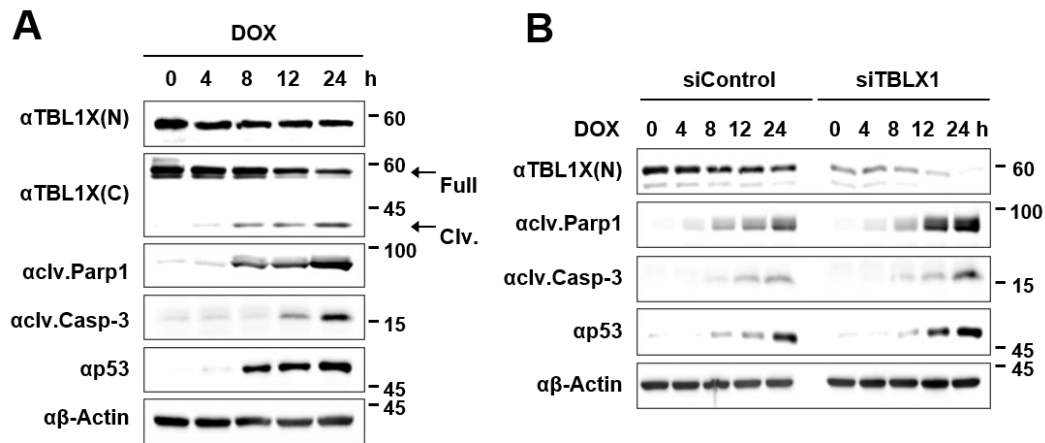


Figure 9. Increased DOX-induced apoptosis in H9c2 cells with TBL1X depletion. (A) Endogenous TBL1X was cleaved in a time-dependent manner following DOX treatment. The cells were treated with 2 μ M DOX for the indicated time. Protein from the H9c2 cells was extracted and immunoblotted with the indicated antibodies. (B) Depletion of TBL1X exacerbated the DOX-induced TBL1X cleavage and p53-dependent apoptotic cell death. Either siControl or siTBL1X was transiently transfected in H9c2 cells and treated with 2 μ M DOX for the indicated times. Cells were harvested, and total protein extracted. Whole-cell lysates were immunoblotted with the indicated antibodies. si-: siRNA. N: N-terminus.

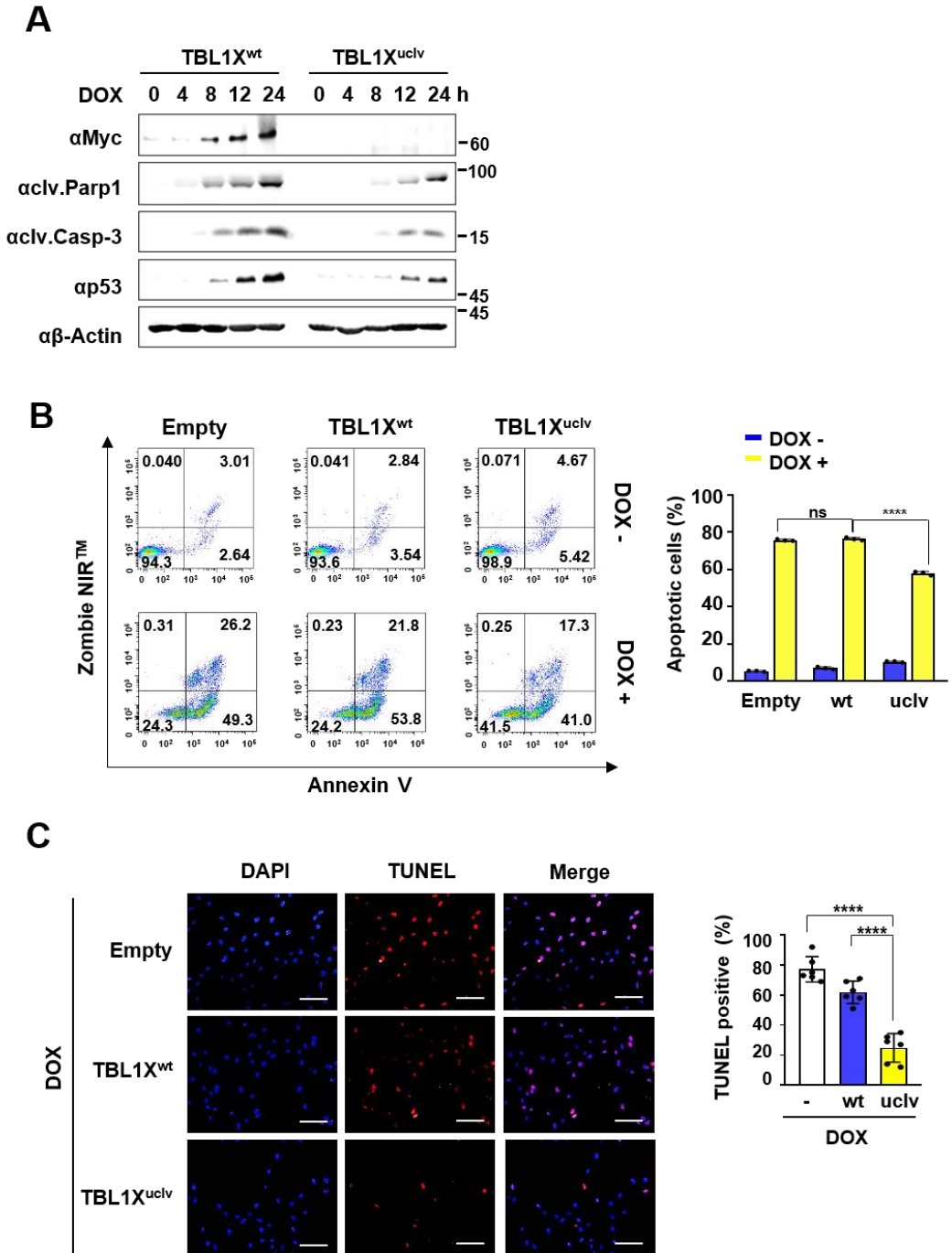


Figure 10. Inhibition of TBL1X cleavage can mitigate the increase in DOX-induced apoptosis. (A) Abrogation of TBL1X cleavage decreased the expression of apoptotic proteins in response to the DOX treatment. Either TBL1X^{WT} or TBL1X^{uclv} construct was transfected into H9c2 cells, and the cells were exposed to 2 μ M DOX for 24 h. (B) Annexin V-positive cells were assessed by flow cytometry. Cells were exposed to 2 μ M DOX for 24 h. A representative image of three independent experiments is shown (right panel). The histogram depicts the quantification of apoptosis (in percentage; Annexin V and Zombie NIR-dual positive cells with or without DOX treatment for TBL1X^{WT} and TBL1X^{uclv} (left panel). (C) Representative image of TUNEL-positive apoptotic cells (red) versus DAPI (blue). Total cells positive for Empty, wild-type TBL1X, and uncleaved-TBL1X mutant overexpression were detected by fluorescent microscopy. Cells were exposed to 2 μ M DOX for 24 h. Representative images of three independent experiments are demonstrated (right panel). Scale bar = 20 μ m. The histogram depicts the quantification of apoptosis (in percentage; the total number of TUNEL-positive cells versus DAPI-positive cells) for TBL1X^{WT} and TBL1X^{uclv}. The values are presented as the mean \pm S.D. from three independent experiments. n.s., no significance. **** $p < 0.0001$ (Student's *t*-test).

5. DOX-induced TBL1X cleavage blocks the Wnt/ β -catenin signaling pathway in H9c2 cells

To demonstrate that Wnt/ β -catenin pathway reduces DOX-induced cardiomyocytes apoptosis, the additional TUNEL staining was conducted. Wnt agonist treatment, LiCl and CHIR99021, DOX-induced apoptotic cell death was remarkably decreased (Figure 11). The results are also supported by previous literatures^{13,14,32}. Based on the result, it was hypothesized that DOX-induced TBL1X cleavage would inhibit the Wnt/ β -catenin signaling axis. The major factors involved in the pathway following the TBL1X knockdown were monitored to test this. The depletion of TBL1X significantly reduced the levels of Wnt target genes *Axin2* and *c-myc* in response to the DOX treatment (Figure 12A). The IP and PLA analyses showed that the TBL1X^{uclv}- β -catenin complex was not affected by the DOX treatment (Figure 12B, C). It was assumed that these binding differences would be seen because the cellular localization of the two proteins, TBL1X and β -catenin, respectively, changed during the DOX treatment. TBL1X^{WT} was translocated to the cytosol, but TBL1X^{uclv} was still localized in the nucleus in response to the DOX (Figure 13A). Immunostaining was then conducted to determine whether the DOX treatment affects the nuclear translocation of β -catenin. Notably, the DOX treatment induced the nuclear localization of β -catenin in a dose-dependent manner (Figure 13B, left panel), and this was further confirmed by cell fractionization (Figure 13B, right panel). TBL1X has been shown to be recruited to the TCF binding sites alongside β -catenin to activate Wnt targets, such as

Axin2 and *c-Myc*^{23,24}. Consequently, we investigated whether β -catenin occupancy in the loci of Wnt target genes, specifically *Axin2* and *c-Myc*, was affected by TBL1X cleavage after DOX exposure. The chromatin immunoprecipitation (ChIP) assay revealed that β -catenin occupancy becomes significantly higher in TBL1X^{uclv}-overexpressing cells than in TBL1X^{WT}-overexpressing cells in the presence of DOX (Figure 14A). Concordantly, uncleaved-TBL1X expression significantly increased Wnt reporter activity even in the presence of DOX (Figure 14B). Furthermore, the cleaved-TBL1X following DOX treatment expected to undergo ubiquitin-dependent proteasomal degradation. So, i believe that the cleaved-TBL1X will not be able to maintain the functional properties of intact TBL1X. As a result, TBL1X mutants which were truncated at cleavage site failed to increase in both Wnt reporter activity and *Axin2* mRNA expression (Figure 15). These results suggest that TBL1X cleavage decreases Wnt/ β -catenin activity through its dissociation from β -catenin and that the attenuation leads to apoptotic cell death by enhancing the sensitivity to DOX.

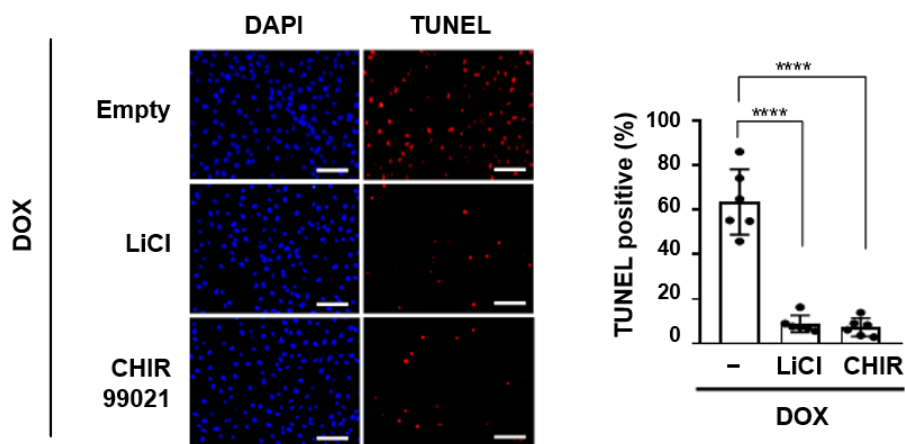
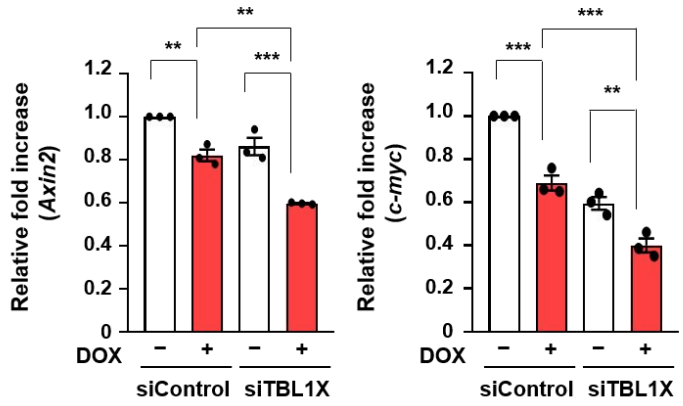
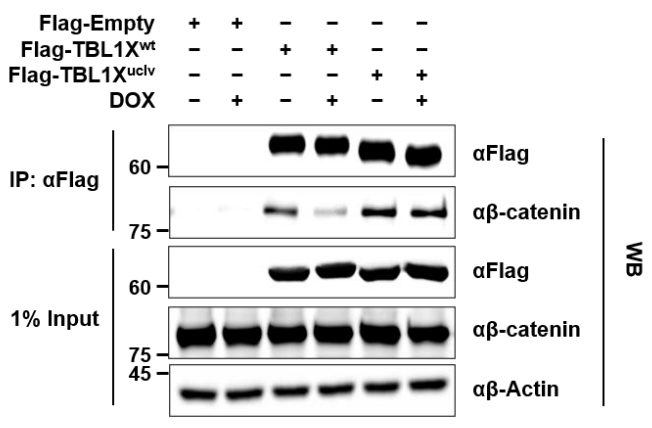


Figure 11. Activation of the Wnt/ β -catenin signaling pathway inhibits DOX-induced apoptosis. H9c2 cells were exposed to LiCl (2.5 mM) or CHIR99021 (3 μ M), Wnt agonist, in the present of DOX for 24 h. Representative image of TUNEL-positive apoptotic cells (red) versus DAPI (blue). Scale bar = 20 μ m. The histogram depicts the quantification of apoptosis (in percentage; the total number of TUNEL-positive cells versus DAPI-positive cells). The values are presented as the mean \pm S.D. from three independent experiments. **** $p < 0.0001$ (Student's t-test). LiCl: lithium chloride, TUNEL: Terminal deoxynucleotidyl transferase dTUP nick and labeling.

A



B



C

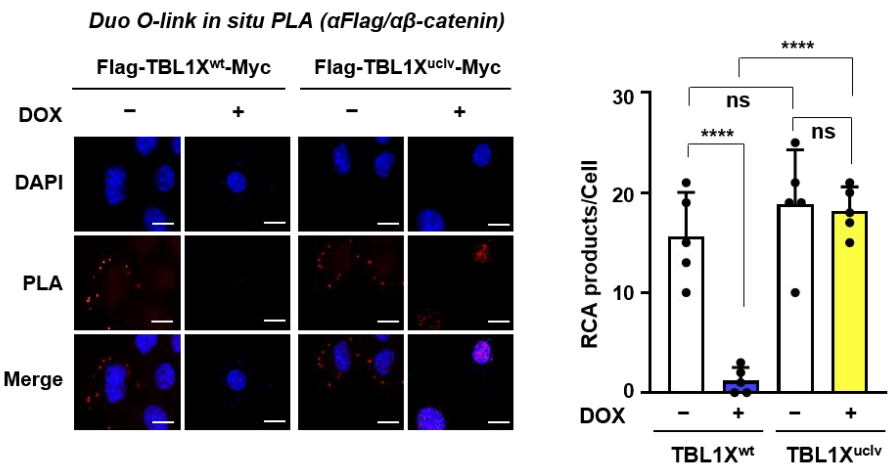


Figure 12. Inhibition of TBL1X cleavage can alleviate the decrease in DOX-induced reduction of the Wnt/ β -catenin signaling pathway. (A) *TBL1X* knockdown decreased mRNA expression of the Wnt target genes. H9c2 cells were transfected with either siControl or siTBL1X and exposed to 1 μ M DOX for 24 h. cDNA was synthesized from mRNA, and the levels of *Axin2* and *c-Myc* were analyzed using real-time PCR. (B) Exogenous overexpressed TBL1X^{WT} was dissociated from β -catenin following the DOX treatment. The indicated plasmid was transfected with or without 1 μ M DOX for 24 h in H9c2 cells. Whole-cell lysates were immunoprecipitated with a β -catenin antibody and sequentially immunoblotted with the indicated antibodies. (C) *In situ* PLA assay demonstrating the dissociation of cleaved-TBL1X^{WT} from β -catenin in response to DOX. Flag-TBL1X^{WT} or -TBL1X^{uclv} plasmid was overexpressed with or without 2 μ M DOX for 24 h in H9c2 cells. Permeabilized cells were incubated with antibodies against Flag and β -catenin, and the PLA probes were added. The cell nuclei were counterstained with DAPI (blue). Positive signals were analyzed using confocal microscopy. Red dots indicate the TBL1X- β -catenin complex. Representative images of four independent experiments are demonstrated. Scale bar = 50 μ m (left panel). The numbers of RCA products per cell from those images are shown in the bar graph (right panel). si-: siRNA. WB: western blotting. IP: immunoprecipitation. RCA: rolling circle amplification.

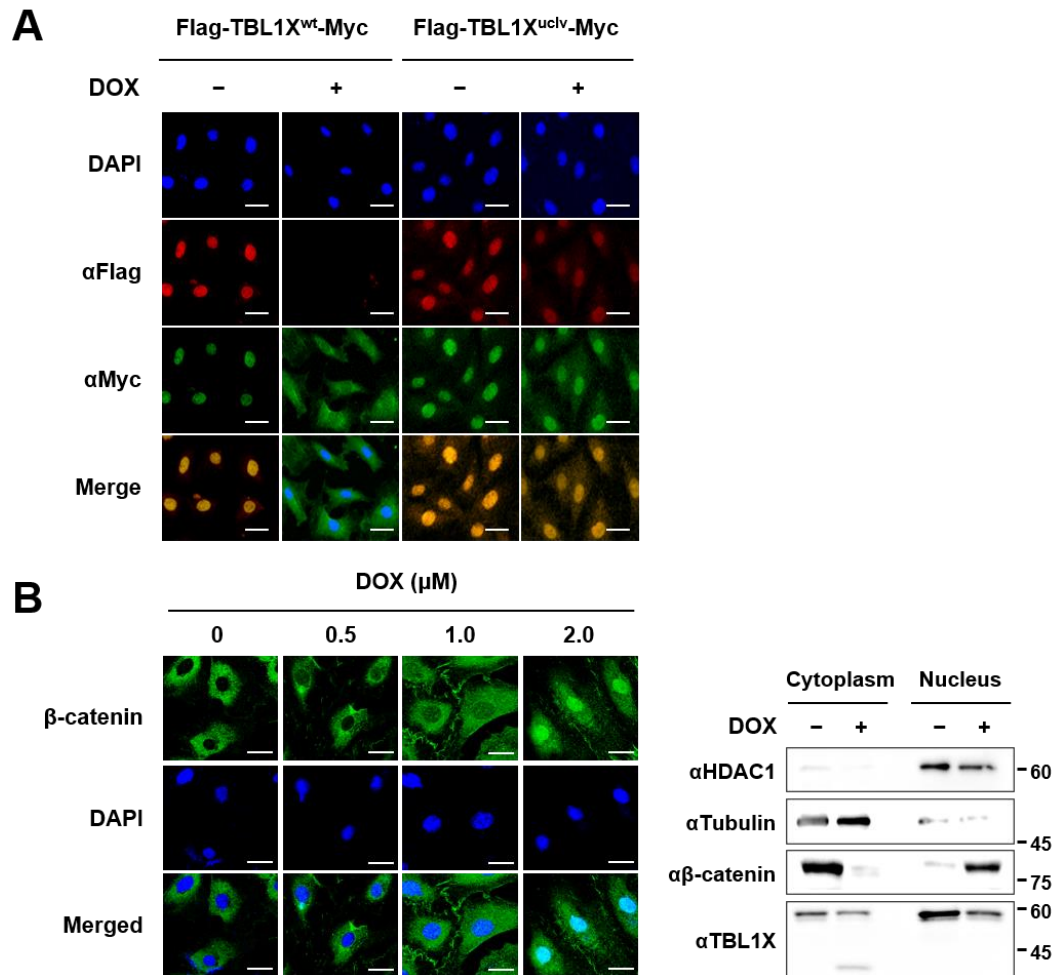


Figure 13. DOX-induced TBL1X cleavage mediates its abnormal subcellular localization and induces nuclear translocation of β-catenin. (A) DOX-induced TBL1X cleavage mediates its abnormal localization. The cleaved TBL1X^{WT} was re-localized into the cytosol in response to the DOX treatment. Flag-TBL1X^{WT}-Myc or Flag-TBL1X^{uclv}-Myc plasmid was transfected into H9c2 cells with or without 1 μM DOX for 24 h. Immunofluorescence analysis was performed as described in the Materials and Methods

section. Representative images of three independent experiments are shown. Scale bar = 50 μm . (B) DOX induces β -catenin nuclear translocation. Cells were treated with 2 μM DOX for the indicated time. H9c2 cells were analyzed using immunofluorescence staining. Representative images of four independent experiments are demonstrated. Scale bar = 50 μm . H9c2 cells with or without 2 μM DOX for 24 h were fractionized into the cytosol and nucleus and used for western blot assays (lower panel).

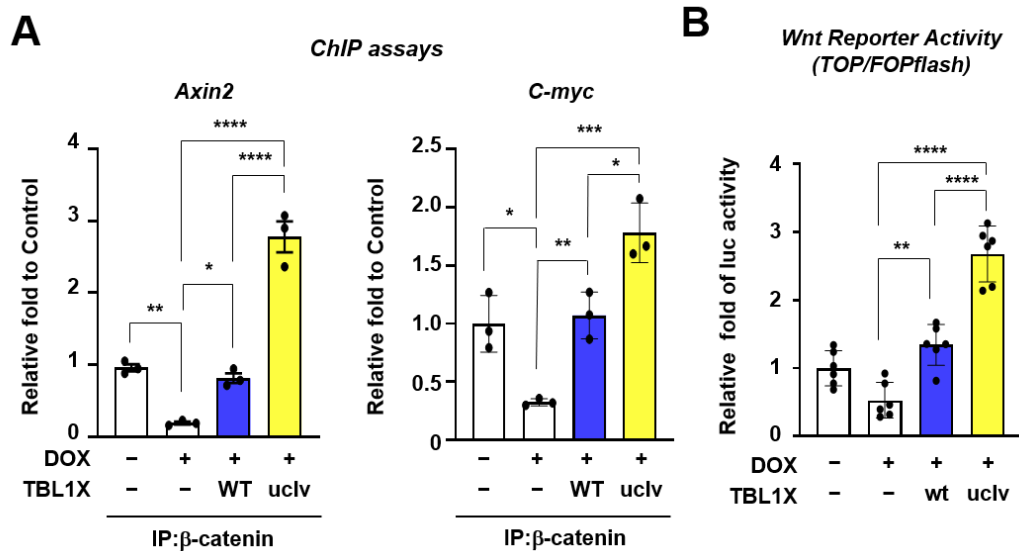


Figure 14. Enhanced occupancy of WNT target gene promoters by TBL1X^{uclv} compared to TBL1X^{WT} under DOX treatment. (A) DOX-induced TBL1X cleavage abrogates its occupancy in the promoter region of Wnt target genes. H9c2 cells were transiently transfected with either the TBL1X^{WT} or TBL1X^{uclv} plasmid with or without 1 μ M DOX for 24 h. Chromatin immunoprecipitation assays were performed with the indicated antibodies. Precipitated samples were analyzed using real-time PCR. (B) Overexpression of TBL1X^{uclv} enhances β -catenin-mediated transcription activity under DOX-exposed conditions. H9c2 cells were co-transfected with TOP/FOPFLASH reporter and the indicated TBL1X plasmid for 24 h. Whole-cell lysates were used for luciferase assays. The results are represented as the mean \pm S.D. from the three independent experiments. n.s., no significance. * $p < 0.05$, ** $p < 0.01$, *** $p < 0.001$, and **** $p < 0.0001$ (Student's t -test).

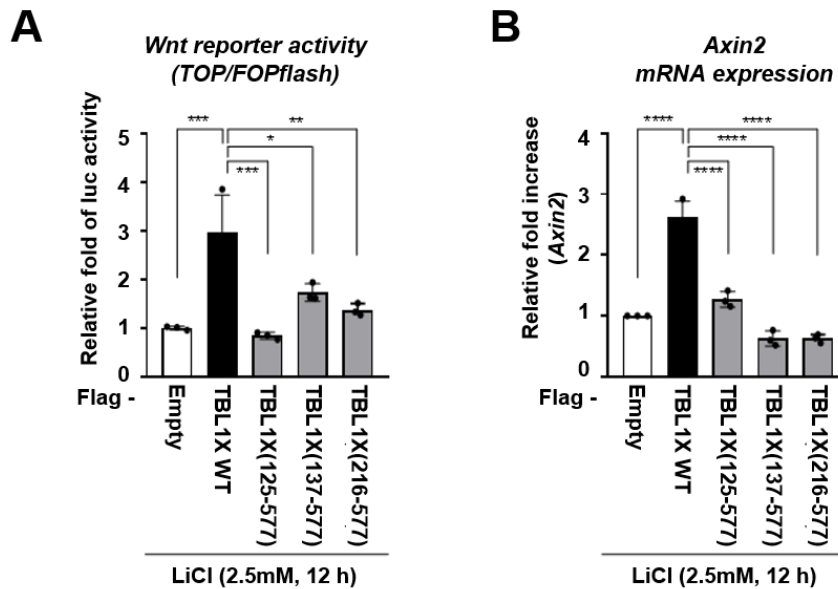


Figure 15. Effects of TBL1X constructs on WNT activity in H9c2 cells under LiCl treatment. (A) The indicated various TBL1X constructs with TOP/FOPFlash reporter were co-transfected in H9c2 cells for 48 h under LiCl-exposed condition. Whole-cell lysates were used for luciferase assays. The results are represented as the mean \pm S.D. from the three independent experiments. * $p < 0.05$, ** $p < 0.01$, *** $p < 0.001$, and **** $p < 0.0001$ (Student's t-test). (B) TBL1X mutants fail to increase in Axin2 mRNA expression. The indicated various TBL1X constructs were transfected in H9c2 cells for 48 h under LiCl-exposed condition. cDNA was synthesized from mRNA, and the levels of Axin2 was analyzed using real-time PCR. **** $p < 0.0001$ (Student's t-test).

6. DOX-induced TBL1X cleavage disrupts spontaneous electrophysiological responses in hiPSC-CMs

To determine whether DOX-induced TBL1X cleavage affects human cardiomyocyte function, human induced pluripotent stem cell-derived cardiomyocytes (hiPSC-CMs) were utilized. hiPSC-CMs are extensively utilized in various fields, including basic research and preclinical safety pharmacology, significantly advancing knowledge of human heart physiology, pathology, and pharmacology. The hiPSCs were cultured in defined media and differentiated into cardiomyocytes (Figure 16). For the molecular and structural characterization of the hiPSC-CMs, they were stained using antibodies against Troponin T2, cardiac type (TNNT2), NK2 Homeobox 5 (NKX2.5), α -actin, titin, and Myosin light chain 2, ventricular type (MLC2V). First, we confirmed that the phenomenon of TBL1X cleavage was also observed in hiPSC-CMs in response to DOX, which was in agreement with our previous findings (Figure 17A).

There are numerous reported assays to measure excitation-calcium-contraction cycle parameters in iPSC-CMs³³. For electrophysiological tests, traditional patch clamp approaches are common, but higher throughput is achieved using multi-electrode arrays (MEAs) in multiwell plates^{34,35}. The MEA approach measures integrated ion channel activity in a contractile context, and is being used by the Comprehensive individualized Process Analysis (CiPA) initiative to conduct *in vitro* drug proarrhythmia risk assessment.

The functional analysis of the hiPSC-CMs was performed on a multi-electrode array

(MEA) system, which provides non-invasive data recordings. The hiPSC-CMs were cultured with or without the inoculation of adenoviruses (Ad-) harboring either TBL1X^{WT} or TBL1X^{uclv} on MEA plates. Data were acquired on the same plate after 9 and 10 days. Similarly, hiPSC-CMs expressing TBL1X^{uclv} had a lower TUNEL positive rate than cells expressing TBL1X^{WT} (Figure 17B).

The MEA-based functionalities of the hiPSC-CMs expressing TBL1X were then investigated. Field potential duration (FPD) record data showed clearly visible R/Q and T peaks with high signal to baseline ratios in cells expressing TBL1X^{WT} or TBL1X^{uclv} with/without DOX. QT interval prolongation was, however, lower with TBL1X^{uclv} than with TBL1X^{WT} under the DOX treatment (Figure 18A). With the DOX treatment, TBL1X^{WT}-expressing cells had a lower spike amplitude, fewer active electrodes and slower conduction velocity than TBL1X^{uclv}-expressing cells (Figure 18B). Beat period and beat period irregularity values were also improved in TBL1X^{uclv}-expressing cells (Figure 18C).

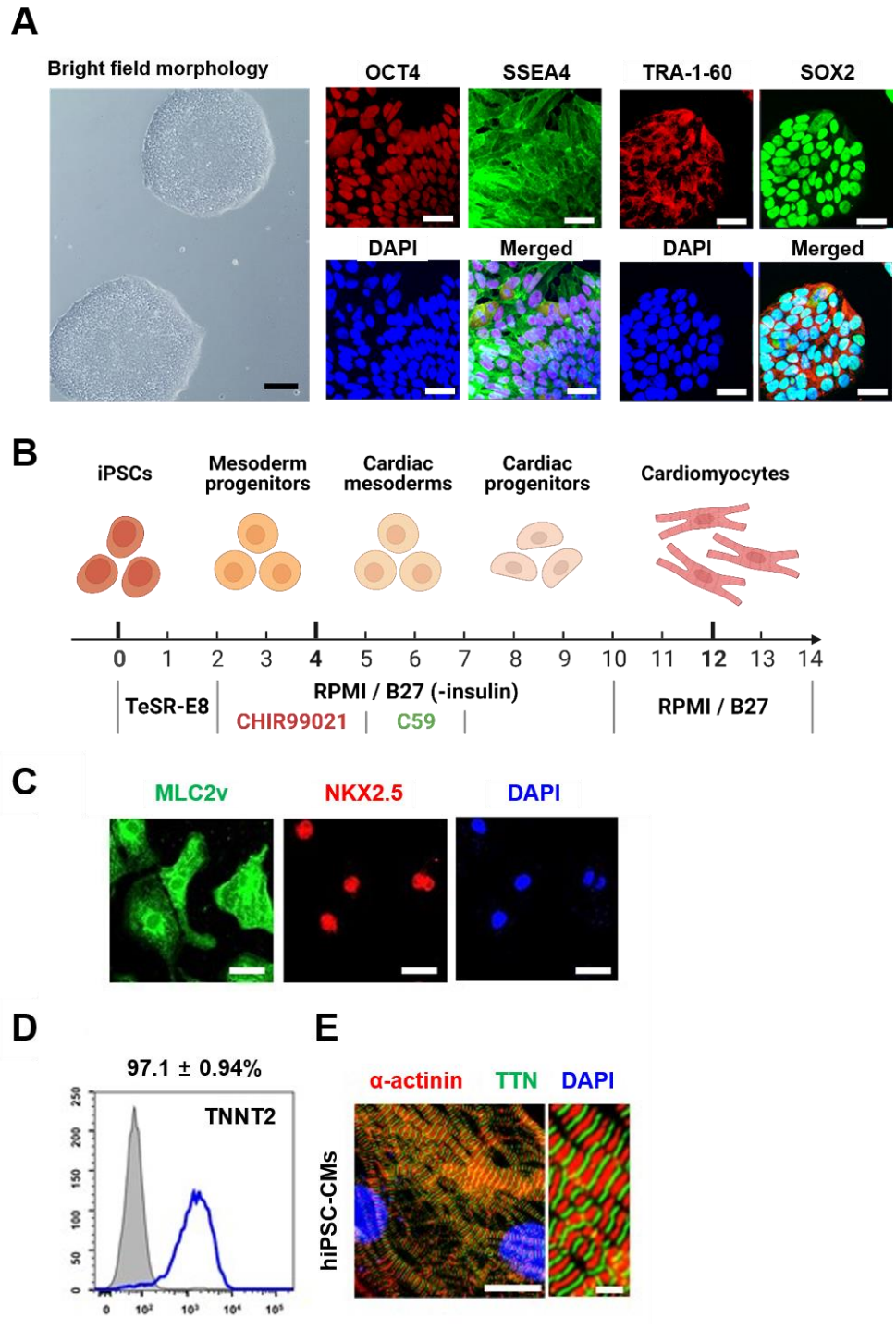


Figure 16. Validation of human induced pluripotent stem cells (hiPSCs) and hiPSC-derived cardiomyocytes (hiPSC-CMs). (A) To validate hiPSC, hiPSC markers, SSEA4, OCT4, TRA-1-60, and SOX2, were immunostained as described in the Materials and Methods section. Representative images of three independent experiments are shown. Scale bar = 50 μ m. (B) Schematic representation of the hiPSC-CMs differentiation. The validated hiPSCs were cultured in the indicated media during the differentiation period and finally differentiated to matured hiPSC-CMs through cardiac mesoderm, cardiac progenitors, and immature CMs. Changes in cell morphology according to differentiation are demonstrated. (C) To validate hiPSC-CMs, hiPSC-CMs were stained with the indicated antibodies recognizing hiPSC-CM markers, and immunofluorescence was analyzed as described in the Materials and Methods (upper right panel). Scale bar = 50 μ m. (D) TNNT2-positive cells were assessed using flow cytometry (lower right panel). (E) To confirm hiPSC-CM, hiPSC-CMs were stained with the MLC2V (ventricular) and TNNT2 antibodies, and immunofluorescence analysis was performed. Scale bar = 50 μ m.

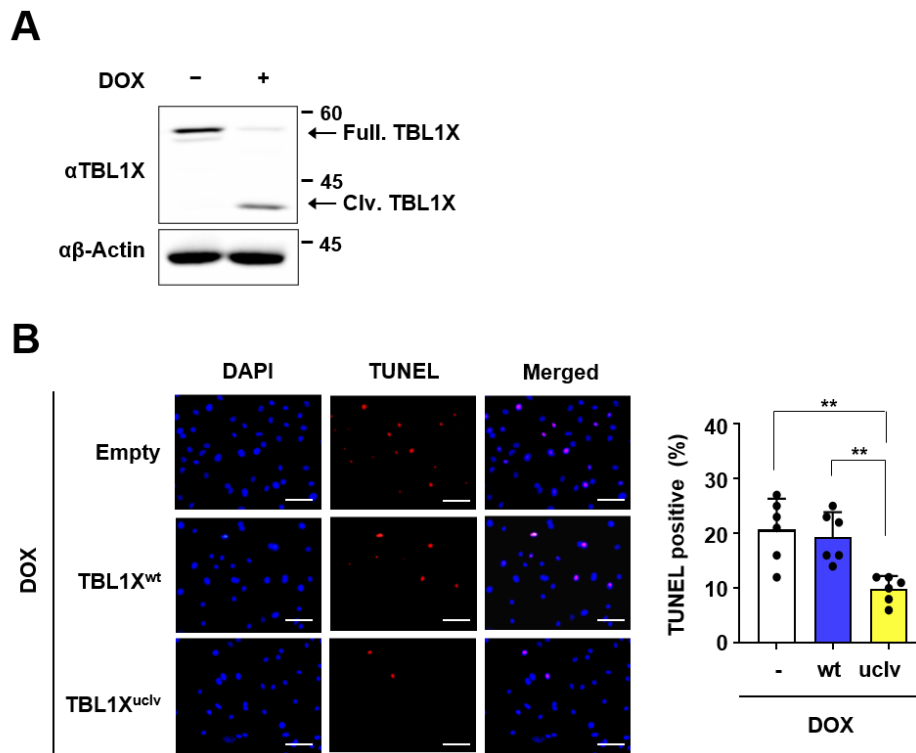


Figure 17. Inhibition of TBL1X cleavage attenuates DOX-induced apoptosis in hiPSC-CMs. (A) iPSC-CMs were cleaved following DOX treatment. iPSC-CMs were treated with 2 μ M DOX, and total proteins were extracted and immunoblotted with the indicated antibodies. (B) Representative image of TUNEL-positive apoptotic cells (red) versus DAPI (blue). Ad-Empty, -TBL1X^{WT}, or Ad-TBL1X^{uclv} inoculated into iPSC-CMs and TUNEL-positive cells were detected using fluorescent microscopy. Cells were exposed to 2 μ M DOX for 24 h. Representative images of three independent experiments are demonstrated (right panel). Scale bar = 20 μ m. The histogram depicts the quantification of apoptosis (in percentage; the total number of TUNEL-positive cells versus DAPI-positive cells) for TBL1X^{WT} and TBL1X^{uclv}.

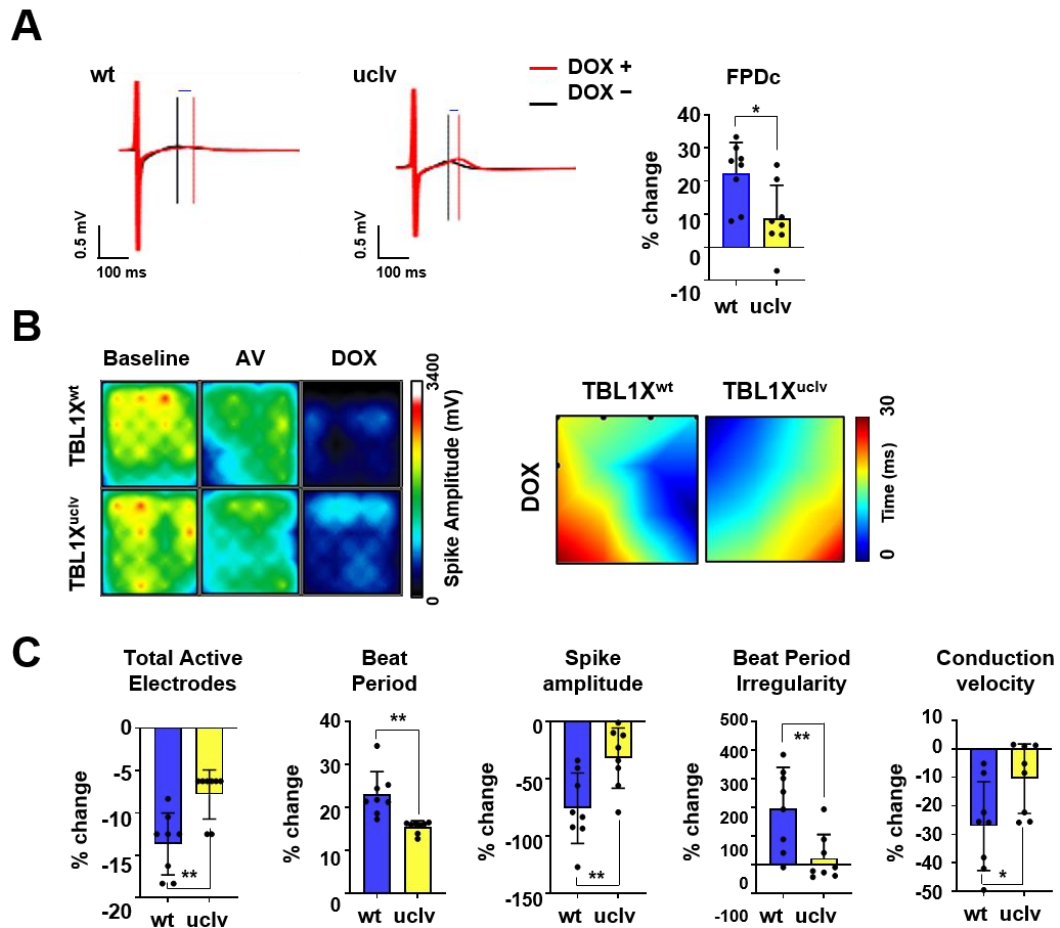


Figure 18. Reduced abnormal electrophysiological phenotypes induced by DOX in hiPSC-CMs treated with TBL1X^{uclv}. (A) Overexpression of Ad-TBL1X^{uclv} in hiPSC-CMs improves field potential in response to DOX. Field potential traces data recorded with the MEA exhibiting mean spontaneous beating trace. Representative trace images recorded with the MEA exhibiting a field potential trace in hiPSC-CMs with the overexpression of Ad-TBL1X^{WT} and Ad-TBL1X^{uclv} with or without DOX. The graph indicates beat period

and spike amplitude. (B) Overexpression of Ad-TBL1X^{uclv} in hiPSC-CMs improves decreased spike amplitude in response to DOX. An active map through the total active lid count is shown. The red and blue colors indicate higher and lower spike amplitudes for iPSC-CMs, respectively. Representative images are presented after three independent experiments. (C) Overexpression of Ad-TBL1X^{uclv} in hiPSC-CMs improves decreased conduction velocity in response to DOX. Conduction plot showing propagation delay of hiPSC-CMs with Ad-Flag-TBL1X^{WT} or Ad-Flag-TBL1X^{uclv}, the blue region represents the origin of the beat (start electrode). Different colors exhibit propagation delay time, as shown in the scale bar. Representative images are demonstrated after three independent experiments (left panel). The data with percent changes compared to that of the baseline were measured using MEA (right panel). % change; % change from baseline = $(100 \times (\text{comparison} - \text{baseline})/\text{baseline})$

7. DOX-induced TBL1X cleavage disrupts calcium homeostasis in hiPSC-CMs

Alterations in EC-coupling and Ca^{2+} handling are directly associated with cardiac injury during heart failure, contributing to ventricular dysfunction and arrhythmia³⁷. Given the strong correlation between cardiac contractile dysfunction and changes in intracellular Ca^{2+} handling, particularly the release of Ca^{2+} from the sarcoplasmic reticulum (SR), systolic Ca^{2+} release was analyzed by measuring Ca^{2+} transients. Representative line-scan Ca^{2+} images obtained from Rhod-2 AM loaded cardiomyocytes correspond to TBL1X^{WT} and TBL1X^{uclv}. The analysis revealed that the amplitude of intracellular Ca^{2+} transients (measured as the peak F/F_0) was significantly lower in cardiomyocytes treated with TBL1X^{WT} than TBL1X^{uclv} (Figure 19A). The time to baseline 50% in cardiomyocytes was significantly shorter in TBL1X^{uclv} than TBL1X^{WT}, indicating a faster decay. These effects on Ca^{2+} kinetics suggest a decline in the systolic Ca^{2+} peak, with prolongation of the duration of systolic Ca^{2+} transients and compromised re-pumping of Ca^{2+} back into the SR with DOX treatment, and the decline recovered significantly after TBL1X^{uclv} overexpression. Additionally, the frequency of Ca^{2+} was significantly higher in TBL1X^{uclv} than TBL1X^{WT} (Figure 19B). These results suggest that inhibiting TBL1X cleavage alleviates some of the abnormal electrophysiological changes occurring in DICT.

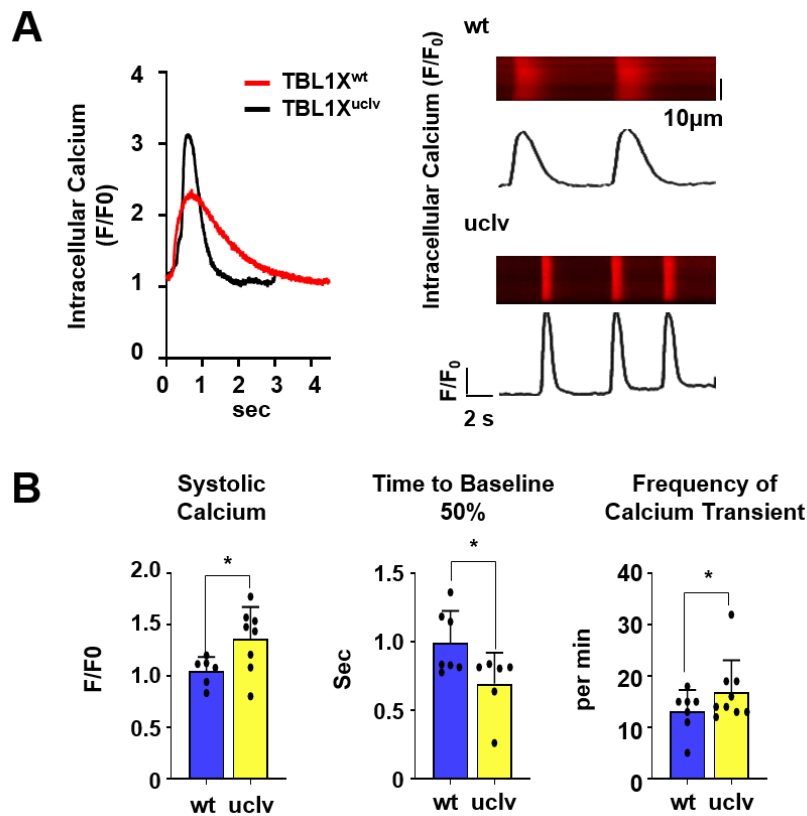


Figure 19. Attenuation of abnormal Ca^{2+} flux induced by DOX in hiPSCs treated with $\text{TBL1X}^{\text{uclv}}$ compared to TBL1X^{WT} . (A) A typical line scan (X-T mode) image of spontaneous calcium transients was obtained. (B) The systolic calcium (F/F_0), time to baseline 50% (s), calcium amplitude (F/F_0), Tau (s), and frequency of calcium transient (per min) were measured. F/F_0 , fluorescence (F) normalized to baseline fluorescence (F_0); s, seconds. The values are the mean \pm S.D. from three independent experiments. * $p < 0.05$ and ** $p < 0.01$ (Student' *t*-test).

8. Inhibiting TBL1X cleavage improves cardiac function and ameliorates cardiac fibrosis in mice

A DICT mouse model was utilized to validate the *in vitro* findings *in vivo*. As previously studied, there is no doubt that repeated intraperitoneal DOX injections represent one of the most validated rodent models of heart failure progressing to DCM^{28,38-42}. To do this, 5 mg/kg of DOX was intraperitoneally injected four times at a cumulative dose of 20 mg/kg after an intramyocardial injection of adeno-associated virus 9 (AAV9) bearing either wild-type or uncleaved-TBL1X (Figure 20A). In AAV9-TBL1X^{WT}-injected mice, the DOX treatment significantly reduced cardiac contractility as determined by fractional shortening (FS%) and the ejection fraction (EF%). This effect was significantly attenuated in TBL1X^{uciv}-expressing mice; the LV internal dimensions at diastole (LVIDd) were also shorter than in TBL1X^{WT}-expressing mice (Figure 20B). Given that DOX treatment induces cardiac fibrosis through collagen accumulation⁴³, cardiac fibrosis was analyzed using Masson's trichrome staining (MTS). Notably, collagen accumulation was significantly lower in mice expressing TBL1X^{uciv} (Figure 21A). Likewise, the number of TUNEL-positive cardiomyocytes was significantly decreased in mice expressing TBL1X^{uciv} (Figure 21B). Together, the data suggest that the inhibition of TBL1X cleavage alleviates DOX-induced cardiotoxicity *in vivo*.

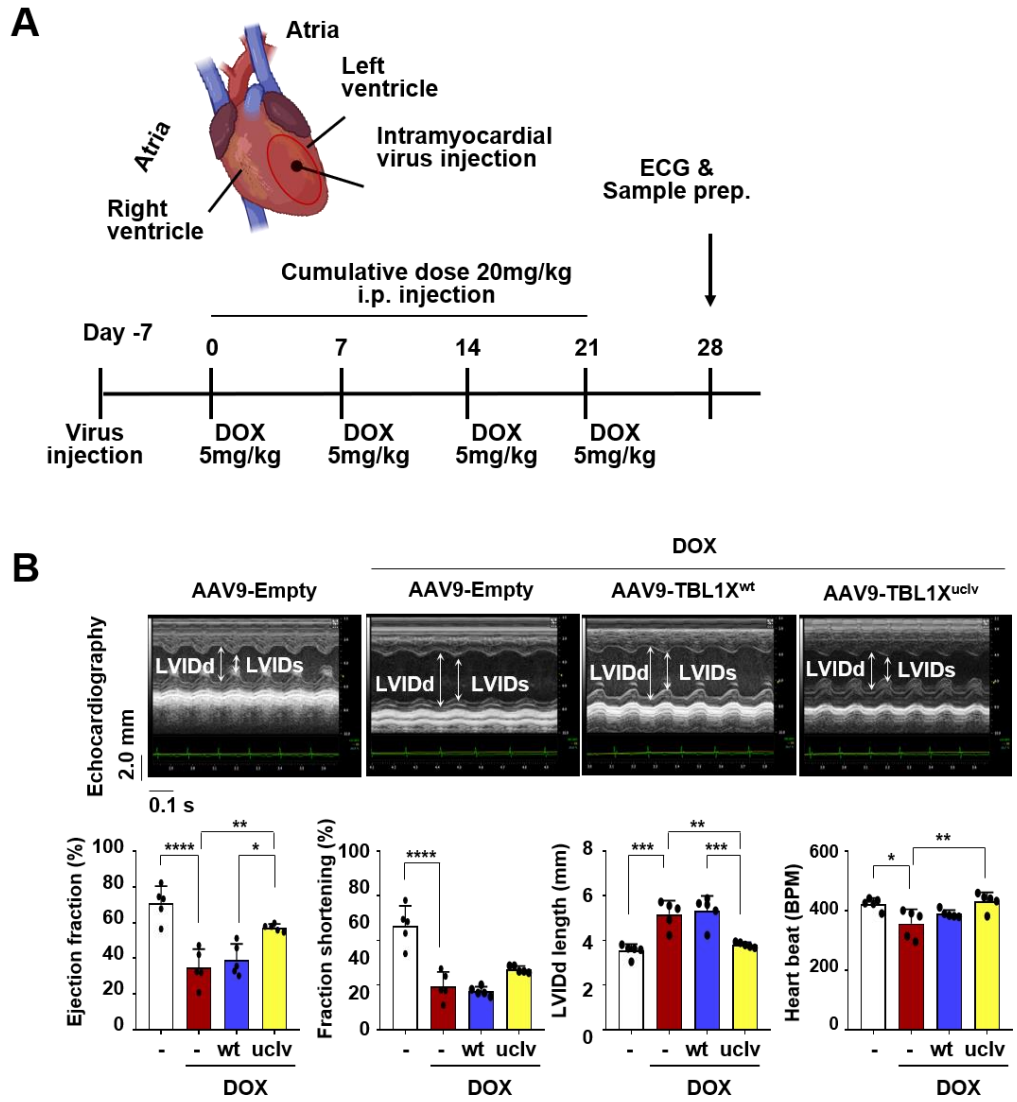


Figure 20. Enhanced cardiac function in a DOX-induced cardiotoxicity mouse model treated with TBL1X^{uclv}. (A) Overexpression of AAV9-TBL1X^{uclv} protects mouse cardiac function against DOX-induced cardiotoxicity. After a week from intramyocardial (i.c.) injection of the indicated viral particle and sequentially intraperitoneal (i.p.) injection of

DOX, mouse cardiac function was observed with echocardiography. Representative M-mode echocardiogram images were demonstrated. LVIDd and LVIDs are marked with a double arrow (upper panel). Ejection fraction%, Fractional shortening%, and LVIDd length were measured. The values are demonstrated as the mean \pm S.E. from three independent experiments. * $p < 0.05$ and ** $p < 0.01$ (Student's t -test; $n = 5$). ECG; electrocardiogram, prep; preparation, i.p.; intraperitoneal, AAV9; Adeno-associated virus, serotype 9, LVIDd; Left ventricular internal dimension at end-diastole, LVIDs; Left ventricular internal dimension at end-systole, BPM; beats per minute.

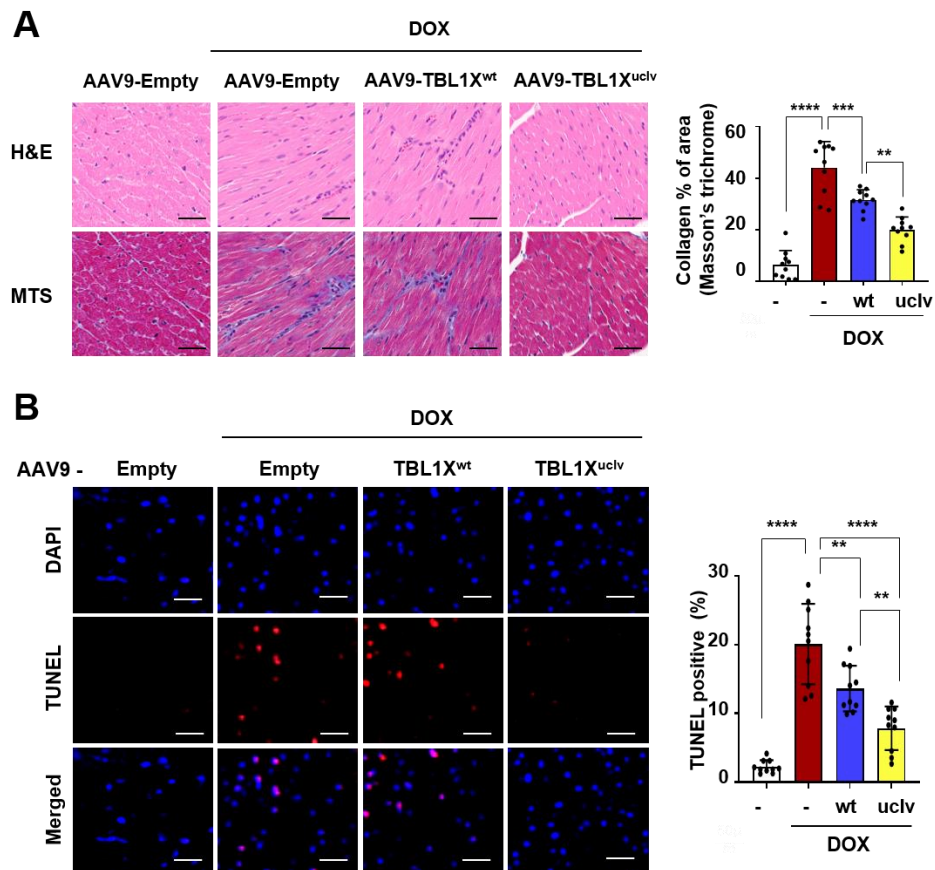
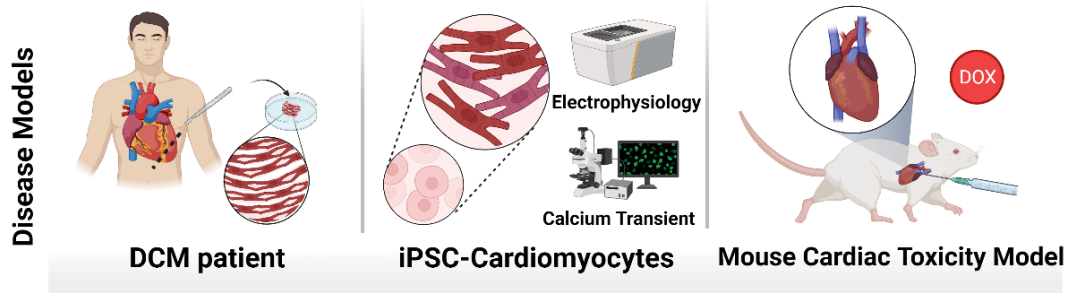


Figure 21. Reduction in inflammation and apoptosis in a mouse model of DOX-induced cardiotoxicity treated with TBL1X^{uclv}. (B) Overexpression of TBL1X^{uclv} inhibits DOX-induced cardiac fibrosis in mice. After echocardiography, mice were sacrificed, and their cardiac tissues dissected. The extent of fibrosis was measured using hematoxylin and eosin (H&E) or Masson's trichrome staining (MTS). Collagen fibers are shown in blue. Two representative images of H&E or MTS staining are demonstrated (left panel). Scale bar = 50 μ m. The percent of the collagen-stained area was calculated

immunohistochemistry (IHC) profiler plugin in ImageJ software. (right panel). The values are the mean \pm S.E. from three independent experiments ($n = 5$). ** $p < 0.01$, and **** $p < 0.0001$ (Student' t -test). (C) Inhibition of TBL1X cleavage suppresses mouse cardiomyocyte death. After echocardiography, mice were sacrificed, and their cardiac tissues dissected. DNA damage in the paraffin-embedded cardiac tissues caused by DOX-induced cardiotoxicity was determined using TUNEL assays. The values are represented as the mean \pm S.E. from three independent experiments. * $p < 0.05$ and **** $p < 0.0001$ (Student's t -test). Scale bar = 50 μm .



Doxorubicin-induced Cardiotoxicity

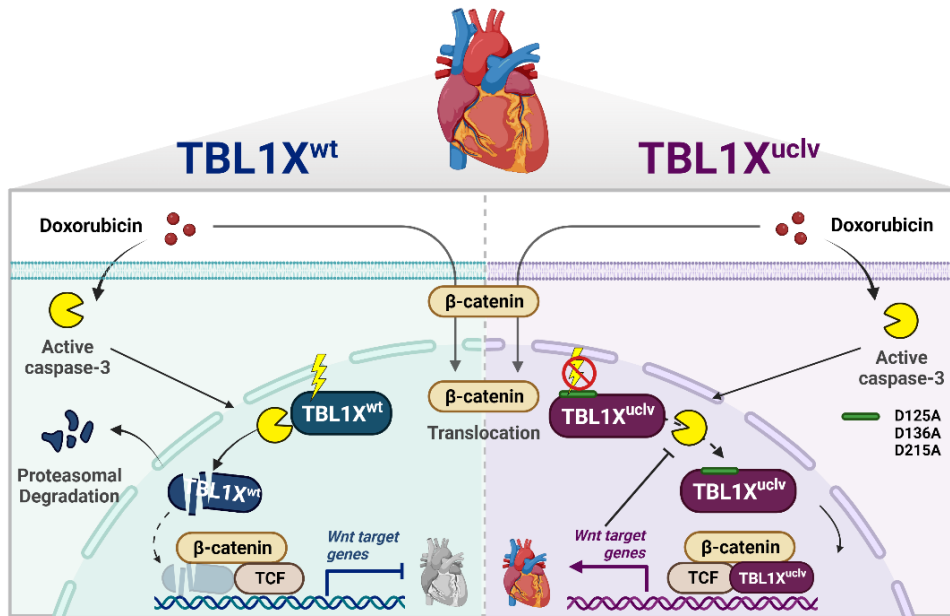


Figure 22. Alleviation of DOX-induced cardiotoxicity through inhibition of TBL1X cleavage. Abbreviations: DCM, dilated cardiomyopathy; iPSC, induced pluripotent stem cell; DOX, doxorubicin; D, aspartate; A, alanine; TBL1X, transducin beta like 1 X-linked; WT, wild type; uclv, uncleaved form; TCF, T-cell factor.

IV. DISCUSSION

Anthracyclines are crucial to many chemotherapy regimens but are also linked to an elevated risk of cardiomyopathy, culminating in heart failure. In this regard, it is necessary to elucidate their molecular mechanisms and identify effective preventive and therapeutic targets of Doxorubicin-induced cardiotoxicity (DICT). In this study, we have demonstrated that inhibiting TBL1X cleavage reduced the DOX-induced death of the cardiomyocytes. More importantly, wild-type TBL1X (TBL1X^{WT}) failed to activate Wnt/ β -catenin signaling despite β -catenin nuclear translocation following DOX administration, but uncleavable variant of TBL1X (TBL1X^{uclv}) efficiently activated Wnt/ β -catenin signaling, highlighting the importance of TBL1X cleavage and its functions during cardiomyocyte apoptosis. Moreover, this study delineates the biological and mechanistic relevance of TBL1X cleavage within the context of DICT, employing an integrative approach encompassing *in vitro*, *in vivo*, and *ex vivo* methodologies to elaborate the molecular dimensions and therapeutic implications thereof.

Evidence has shown beyond a doubt that a proteolytic cleavage precipitates protein destabilization. Specifically, cleavage of the gene associated with retinoid interferon-induced mortality (*Grim*) at aspartate 136 was found to enhance the stability of *Grim* by removing the lysine residue for ubiquitin conjugation, thereby altering its degradation pathway⁴⁴. Conversely, caspase-3-mediated cleavage of histone deacetylase 3 (HDAC3) cleavage at aspartate 391 was found to ultimately lead to its degradation in etoposide-

induced genotoxic stress⁴⁵. Several post-translational modifications (PTMs) of TBL1X including phosphorylation⁴⁶ and sumoylation²⁴ have already been reported; however, in this investigation, we have demonstrated its cleavage in DICT for the first time. There is a large amount of evidence showing that protein cleavage, a PTM, induces protein degradation^{47,48}. Considering the mRNA expression profiles of TBL1X in cardiac tissues, the diminished expression of TBL1X in dilated cardiomyopathy (DCM) patients might be attributed to cleavage-induced degradation. Our observations reveal that DOX triggers TBL1X cleavage at aspartate residues 125, 136, and 215 in a caspase-3-dependent manner, leading to its ubiquitin-dependent degradation, thereby providing a plausible mechanistic insight into TBL1X regulation and its potential implications in cardiac pathology.

Remarkably, the overexpression of the uncleavable TBL1X variant (TBL1X^{uclv}) inhibited ubiquitin-mediated proteasomal degradation of TBL1X, thereby conferring enhanced stabilization relative to the wild-type TBL1X (TBL1X^{WT}) in the wake of DOX exposure. The Lis-homology (LisH) domain in the N-terminal plays a crucial role in the maintenance of protein stability⁴⁹ and is located within the 55–87 amino acid range of TBL1X, which is important for its half-life⁵⁰. Our findings suggest that the proteolytic cleavage of TBL1X culminates in the excision of the LisH domain, thereby facilitating its ubiquitin-dependent proteasomal degradation and ostensibly abbreviating its half-life. Additionally, the differential presentation of endogenous TBL1X cleavage products in western blot analyses compared to exogenous TBL1X is likely attributable to the variations in ubiquitin-dependent degradation pathways, underscoring the nuanced regulatory

mechanisms of TBL1X stability.

The question of how TBL1X^{uclv}, which has a stable status despite the DOX-exposed environment, affects cardiomyocytes was then addressed. To answer this question, the alterations in the key factors⁵¹ regulating the death of cardiomyocytes in response to DOX were observed. The data showed a time-dependent increase in p53 and pro-apoptotic proteins with DOX-induced TBL1X cleavage. Interestingly, under DOX exposed conditions, the expression of pro-apoptotic proteins, including p53 and the apoptosis rate in TBL1X^{uclv}-overexpressing H9c2 cells was lower when compared with those in TBL1X^{WT}-overexpressing cells. These results indicate that intact TBL1X, even in DICT, plays a protective role in cardiomyocytes by suppressing p53. The next aim was to identify which molecular mechanisms were involved in cardiomyocyte death in DICT. The inhibition of Wnt/ β -catenin signaling promotes DOX-triggered apoptosis⁵². DOX induces cardiotoxicity by inhibiting the Wnt/ β -catenin signaling pathway^{14,32}. A high level of cross-talk between p53 and Wnt signaling has been revealed⁵³. Specifically, activation of p53, a key regulator of apoptosis signaling, leads to the down-regulation of the Wnt/ β -catenin signaling pathway⁵⁴. Some studies indicate that the loss of p53 results in the activation of the Wnt/ β -catenin signaling pathway^{55,56}. At this time, the regulation of the pathway is determined by the occupancy of p53 at the *Wnt* promoter. Previous findings indicate that the high occupancy of p53 at the site induces the inhibition of the Wnt/ β -catenin signaling pathway. Therefore, it is possible that TBL1X^{uclv}-triggered the reduction of p53 and that this may cause inactivation in the pathway following the DOX treatment. One of the most

important findings was that TBL1X and β -catenin were recruited to the Wnt target genes, *Axin 2* and *c-myc*, leading to Wnt signaling activation^{23,24}. These results indicate that TBL1X can also directly regulate the Wnt/ β -catenin signaling pathway. However, studies on TBL1X-mediated regulation of the Wnt/ β -catenin signaling pathway under cellular damage have not yet been conducted in sufficient detail. Our results show that TBL1X^{uclv} firmly formed a complex with β -catenin in response to DOX.

Furthermore, ChIP assay analyses and reporter gene assays showed that TBL1X^{uclv} dramatically induced the recruitment of β -catenin to the promoter region of *Wnt* target genes, *Axin2* and *c-myc*, and suppressed the decrease in DOX-induced *Wnt* reporter activity. Based on the findings from the immunofluorescence analyses, it is believed that the normal localization of TBL1X^{uclv}, even under the DOX-exposed conditions, plays a decisive role in the above results. TBL1X is predominantly localized in the nucleus^{20,21}. Leu 67 of TBL1X is important for its normal localization⁵⁰. Therefore, considering that the cleaved sites of TBL1X occur in response to DOX, it is somewhat predictable that there will be aberrant re-localization in the cytosol. Moreover, the intracellular location where cleavage of TBL1X occurs in the DICT condition must also be considered. Taking all of the previous findings together, it is reasonable to infer that the cleavage of TBL1X occurred within the nucleus in response to DOX. However, we have deduced that, following the DOX treatment, the LisH domain, including L67 in TBL1X, was lost due to the DICT-triggered cleavage that occurred in the nucleus, and consequently, it was abnormally transferred to the cytosol and was ultimately degraded. Activated caspase-3 is translocated to the nucleus by simple

diffusion and disruption of the cytosol-nuclear barrier for its substrates identified in the nucleus in the progression of apoptosis^{57,58}. Indeed, in the DICT condition, TBL1X is abnormally located in the cytosol due to its active caspase-3-mediated cleavage. In general, damaged proteins with aberrant subcellular localization also target ubiquitin-mediated proteasomal degradation to help maintain proteostasis⁵⁹. In this study, we demonstrated that TBL1X^{uclv} is located in the nucleus despite DOX exposure in H9c2 cells, unlike in TBL1X^{WT}-transfected cells. β -catenin is constantly ubiquitinated in the cytosol under normal conditions, stabilized following Wnt activation, and subsequently translocated to the nucleus⁶⁰. Therefore, for the interactions between intact TBL1X and β -catenin in DICT, the stabilization and nuclear localization of β -catenin should be investigated following DOX treatment. Notably, we observed for the first time that β -catenin expression was increased and translocated to the nucleus in a dose-dependent manner with DOX. After the DOX treatment, the stabilization and translocation of β -catenin are crucial for its complex formation with TBL1X^{uclv}. Synthetically, stabilization and normal localization in the nucleus of TBL1X and translocalization of β -catenin under DOX-exposed conditions seem to play a critical role in protecting cardiomyocytes through activating the Wnt/ β -catenin signaling pathway.

Finally, we introduced both *ex-vivo* (hiPSC-CM) and *in vivo* (mouse) systems to evaluate the effects of intact TBL1X on cardiomyocytes function in the DICT environment. TBL1X cleavage was also observed in hiPSC-CMs following the DOX treatment. In addition, Ad-TBL1X^{uclv} overexpression protected hiPSC-CMs from DOX-induced cardiomyocyte death.

Monitoring cardiomyocytes' electrical activity is crucial to investigating cardiac diseases and developing therapeutic strategies ⁶¹. Our MEA analyses revealed that TBL1X^{uclv} overexpression partially ameliorated the disruption of these electrophysiological factors, such as FPD, total active electrodes, beat period, spike amplitude, and conduction velocity following the DOX treatment ⁶². Furthermore, we elucidated that this phenomenon was because intact TBL1X, even after DOX exposure, controls the disruption of Ca²⁺ homeostasis, a predominant hallmark related to cardiac functionality ⁶³. Current evidence indicates that the diastolic intracellular Ca²⁺ concentration is increased in response to DOX, leading to left ventricular dysfunction ⁶⁴. Our data have shown that the DOX-induced abnormal functional changes in echocardiographic indicators were alleviated in AAV9-TBL1X^{uclv}-overexpressing mouse hearts via intramyocardial injection. Additionally, DOX-induced fibrosis and apoptotic cell death were significantly lower in AAV9-TBL1X^{uclv}-overexpressing mouse cardiac tissues than in AAV9-TBL1X^{WT}-overexpressing tissues.

Irreversible adverse side effects in cancer treatment result in increased patient morbidity and mortality. Cardiotoxicity is the most significant side effect of chemotherapeutic agents. Therefore, "prevention" strategies to avoid it are paramount, and most previous trials have focused on biomarkers ⁶⁵. This study is thus valuable as it expands the selection of preemptive strategies for preventing DICT by presenting a novel target and identifying the molecular mechanisms underlying it.

Despite these advantages, our study has several limitations. First, we did not directly compare the phenomenon of TBL1X cleavage in cardiac tissues between normal

individuals and patients with DCM. We obtained cardiac tissues from 6 patients with DCM but failed to obtain those from normal individuals. Using hiPSC-CMs as a control group was the best option in this situation. Second, based on only the antibodies recognizing the C-terminal of TBL1X [TBL1(C) and Myc] following DOX treatment, detected endogenous and exogenous cleaved bands of TBL1X appear to have differences. This is inferred because endogenous TBL1X, which has a relatively low expression level, was degraded at a faster rate after its cleavage. In addition, differences in cleaved-bands of endogenous TBL1X between hiPSC-CMs and H9c2 cells under the same circumstances are presumed to result from species differences. Finally, as our study focused on the cross-talk between TBL1X and the Wnt/ β -catenin signaling pathway in DICT, direct experimental evidence supporting a correlation between either p53-TBL1X or the p53-Wnt/ β -catenin signaling pathway is currently insufficient. Therefore, more elaborate and in-depth studies are required. Although this study has limitations, it is clear that our findings have suggested a new molecular mechanism underlying DCM and DICT and related preventive-/therapeutic approaches.

V. CONCLUSION

In this investigation, we have identified TBL1X cleavage-induced degradation following DOX exposure and that this process triggers cardiomyocyte death. Specifically, the N-terminus processing of TBL1X by active caspase-3 is crucial for apoptosis induction through the inhibition of Wnt/ β -catenin signaling in cardiomyocytes, and it is effectively reversed by the uncleaved mutant form of TBL1X (TBL1X^{uclv}). These findings were also validated in human induced pluripotent stem cell-derived cardiomyocytes (hiPSC-CMs) and *in vivo* DICT mouse models. The results enhance our understanding of TBL1X function and will aid in developing valuable strategies to alleviate DICT during cancer treatment.

REFERENCES

1. De Angelis A, Urbanek K, Cappetta D, Piegari E, Ciuffreda LP, Rivellino A, et al. Doxorubicin cardiotoxicity and target cells: a broader perspective. *Cardiooncology* 2016;2:1-8.
2. Lefrak EA, Pitha J, Rosenheim S, Gottlieb JA. A clinicopathologic analysis of adriamycin cardiotoxicity. *Cancer* 1973;32:302-14.
3. Zamorano JL, Lancellotti P, Rodriguez Munoz D, Aboyans V, Asteggiano R, Galderisi M, et al. 2016 ESC position paper on cancer treatments and cardiovascular toxicity developed under the auspices of the ESC committee for practice guidelines: The task force for cancer treatments and cardiovascular toxicity of the european society of cardiology (ESC). *Eur Heart J* 2016;37:2768-801.
4. Henriksen PA. Anthracycline cardiotoxicity: an update on mechanisms, monitoring and prevention. *Heart* 2018;104:971-7.
5. Haupt LP, Rebs S, Maurer W, Hubscher D, Tiburcy M, Pabel S, et al. Doxorubicin induces cardiotoxicity in a pluripotent stem cell model of aggressive B cell lymphoma cancer patients. *Basic Res Cardiol* 2022;117:1-24.
6. Strongman H, Gadd S, Matthews A, Mansfield KE, Stanway S, Lyon AR, et al. Medium and long-term risks of specific cardiovascular diseases in survivors of 20 adult cancers: a population-based cohort study using multiple linked UK electronic health records databases. *Lancet* 2019;394:1041-54.
7. Nishi M, Wang PY, Hwang PM. Cardiotoxicity of cancer treatments: Focus on anthracycline cardiomyopathy. *Arterioscler Thromb Vasc Biol* 2021;41:2648-60.

8. Shakir DK, Rasul KI. Chemotherapy induced cardiomyopathy: pathogenesis, monitoring and management. *J Clin Med Res* 2009;1:8-12.
9. Chatterjee K, Zhang J, Honbo N, Karlner JS. Doxorubicin cardiomyopathy. *Cardiology* 2010;115:155-62.
10. Vejpongsa P, Yeh ET. Prevention of anthracycline-induced cardiotoxicity: challenges and opportunities. *J Am Coll Cardiol* 2014;64:938-45.
11. Solem LE, Henry TR, Wallace KB. Disruption of mitochondrial calcium homeostasis following chronic doxorubicin administration. *Toxicol Appl Pharmacol* 1994;129:214-22.
12. Pai SG, Carneiro BA, Mota JM, Costa R, Leite CA, Barroso-Sousa R, et al. Wnt/ β -catenin pathway: modulating anticancer immune response. *J Hematol Oncol* 2017;10:1-12.
13. Cao YJ, Li JY, Wang PX, Lin ZR, Yu WJ, Zhang JG, et al. PKC- ζ aggravates doxorubicin-induced cardiotoxicity by inhibiting Wnt/ β -Catenin Signaling. *Front Pharmacol* 2022;13:1-12.
14. Liang L, Tu Y, Lu J, Wang P, Guo Z, Wang Q, et al. Dkk1 exacerbates doxorubicin-induced cardiotoxicity by inhibiting the Wnt/ β -catenin signaling pathway. *J Cell Sci* 2019;132:1-11.
15. Lorenzon A, Calore M, Poloni G, De Windt LJ, Braghetta P, Rampazzo A. Wnt/ β -catenin pathway in arrhythmogenic cardiomyopathy. *Oncotarget* 2017;8:60640-55.
16. Le Dour C, Macquart C, Sera F, Homma S, Bonne G, Morrow JP, et al. Decreased Wnt/ β -catenin signalling contributes to the pathogenesis of dilated cardiomyopathy caused by mutations in the lamin A/C gene. *Hum Mol Genet* 2017;26:333-43.

17. Kim C, Wong J, Wen J, Wang S, Wang C, Spiering S, et al. Studying arrhythmogenic right ventricular dysplasia with patient-specific iPSCs. *Nature* 2013;494:105-10.
18. Garcia-Gras E, Lombardi R, Giocondo MJ, Willerson JT, Schneider MD, Khoury DS, et al. Suppression of canonical Wnt/ β -catenin signaling by nuclear plakoglobin recapitulates phenotype of arrhythmogenic right ventricular cardiomyopathy. *J Clin Invest* 2006;116:2012-21.
19. Garcia-Pavia P, Kim Y, Restrepo-Cordoba MA, Lunde IG, Wakimoto H, Smith AM, et al. Genetic variants associated with cancer therapy-induced cardiomyopathy. *Circulation* 2019;140:31-41.
20. Yoon HG, Chan DW, Huang ZQ, Li J, Fondell JD, Qin J, et al. Purification and functional characterization of the human N-CoR complex: the roles of HDAC3, TBL1 and TBLR1. *EMBO J* 2003;22:1336-46.
21. Yoon HG, Choi Y, Cole PA, Wong J. Reading and function of a histone code involved in targeting corepressor complexes for repression. *Mol Cell Biol* 2005;25:324-35.
22. Perissi V, Aggarwal A, Glass CK, Rose DW, Rosenfeld MG. A corepressor /coactivator exchange complex required for transcriptional activation by nuclear receptors and other regulated transcription factors. *Cell* 2004;116:511-26.
23. Li J, Wang CY. TBL1-TBLR1 and β -catenin recruit each other to Wnt target-gene promoter for transcription activation and oncogenesis. *Nat Cell Biol* 2008;10:160-9.
24. Choi HK, Choi KC, Yoo JY, Song M, Ko SJ, Kim CH, et al. Reversible SUMOylation of TBL1-TBLR1 regulates β -catenin-mediated Wnt signaling. *Mol Cell* 2011;43:203-16.

25. Matsuzawa SI, Reed JC. Siah-1, SIP, and Ebi collaborate in a novel pathway for β -catenin degradation linked to p53 responses. *Mol Cell* 2001;7:915-26.
26. Yasufumi Katanasaka MN, Yoichi Wunagawa, Yusuke Miyazake, Hiromichi Wada, Koji Hasegawa, Tatsuya Morimoto. TBL1 supresses cardiomyocyte hypertrophy by regulating the interaction between HDAC4 and GATA4. *European Cardiology Review* 2018;13:126.
27. Gao S, Ho D, Vatner DE, Vatner SF. Echocardiography in mice. *Curr Protoc Mouse Biol* 2011;1:71-83.
28. Stoddard MF, Seeger J, Liddell NE, Hadley TJ, Sullivan DM, Kupersmith J. Prolongation of isovolumetric relaxation time as assessed by Doppler echocardiography predicts doxorubicin-induced systolic dysfunction in humans. *J Am Coll Cardiol* 1992;20:62-9.
29. Takemura G, Fujiwara H. Doxorubicin-induced cardiomyopathy from the cardiotoxic mechanisms to management. *Prog Cardiovasc Dis* 2007;49:330-352.
30. Vitale J, Carbone F. Systolic heart failure. *N Engl J Med* 2010;362:1545-6.
31. Halim VA, Garcia-Santisteban I, Warmerdam DO, van den Broek B, Heck AJR, Mohammed S, et al. Doxorubicin-induced DNA damage causes extensive ubiquitination of ribosomal proteins associated with a decrease in protein translation. *Mol Cell Proteomics* 2018;17:2297-308.
32. Hu Y, Guo Z, Lu J, Wang P, Sun S, Zhang Y, et al. sFRP1 has a biphasic effect on doxorubicin-induced cardiotoxicity in a cellular location-dependent manner in NRCMs and Rats. *Arch Toxicol* 2019;93:533-46.
33. Laurila E, Ahola A, Hyttinen J, Aalto-Setälä K. Methods for *in vitro* functional analysis of iPSC derived cardiomyocytes-Special focus on analyzing the

- mechanical beating behavior. *Biochim Biophys Acta* 2016;1863:1864-72.
34. Kussauer S, David R, Lemcke H. hiPSCs derived cardiac cells for drug and toxicity screening and disease modeling: What micro-electrode-array analyses can tell us. *Cells* 2019;8:1-29.
 35. Tertoolen LGJ, Braam SR, van Meer BJ, Passier R, Mummery CL. Interpretation of field potentials measured on a multi electrode array in pharmacological toxicity screening on primary and human pluripotent stem cell-derived cardiomyocytes. *Biochem Biophys Res Commun* 2018;497:1135-41.
 36. Dridi H, Kushnir A, Zalk R, Yuan Q, Melville Z, Marks AR. Intracellular calcium leak in heart failure and atrial fibrillation: a unifying mechanism and therapeutic target. *Nat Rev Cardiol* 2020;17:732-47.
 37. Kansakar U, Varzideh F, Jankauskas SS, Gambardella J, Trimarco B, Santulli G. Advances in the understanding of excitation-contraction coupling: the pulsing quest for drugs against heart failure and arrhythmias. *Eur Heart J Cardiovasc Pharmacother* 2021;7:1-3.
 38. Li F, Leier A, Liu Q, Wang Y, Xiang D, Akutsu T, et al. Procleave: Predicting protease-specific substrate cleavage sites by combining sequence and structural information. *Genomics Proteomics Bioinformatics* 2020;18:52-64.
 39. Liu Y, Zhang W, Hu T, Ni J, Xu B, Huang W. A doxorubicin-induced murine model of dilated cardiomyopathy *In Vivo*. *J Vis Exp* 2020;159:1-8.
 40. Ponzoni M, Coles JG, Maynes JT. Rodent models of dilated cardiomyopathy and heart failure for translational investigations and therapeutic discovery. *Int J Mol Sci* 2023;24:1-23.
 41. Qi Y, Chen J, Duan J, Kang L, Wang K, Chen Z, et al. Major vault protein attenuates

- cardiomyocyte injury in doxorubicin-induced cardiomyopathy through activating AKT. *BMC Cardiovasc Disord* 2022;22:1-11.
42. Wang L, Zhang TP, Zhang Y, Bi HL, Guan XM, Wang HX, et al. Protection against doxorubicin-induced myocardial dysfunction in mice by cardiac-specific expression of carboxyl terminus of hsp70-interacting protein. *Sci Rep* 2016;6:28399:1-14.
 43. Wang S, Wang Y, Zhang Z, Liu Q, Gu J. Cardioprotective effects of fibroblast growth factor 21 against doxorubicin-induced toxicity via the SIRT1/LKB1/AMPK pathway. *Cell Death Dis* 2017;8:1-14.
 44. Yeh TC, Bratton SB. Caspase-dependent regulation of the ubiquitin-proteasome system through direct substrate targeting. *Proc Natl Acad Sci USA* 2013;110:14284-9.
 45. Choi HK, Choi Y, Park ES, Park SY, Lee SH, Seo J, et al. Programmed cell death 5 mediates HDAC3 decay to promote genotoxic stress response. *Nat Commun* 2015;6:7390:1-18.
 46. Perissi V, Scafoglio C, Zhang J, Ohgi KA, Rose DW, Glass CK, et al. TBL1 and TBLR1 phosphorylation on regulated gene promoters overcomes dual CtBP and NCoR/SMRT transcriptional repression checkpoints. *Mol Cell* 2008;29:755-66.
 47. Dong H, Dumenil J, Lu FH, Na L, Vanhaeren H, Naumann C, et al. Ubiquitylation activates a peptidase that promotes cleavage and destabilization of its activating E3 ligases and diverse growth regulatory proteins to limit cell proliferation in *Arabidopsis*. *Genes Dev* 2017;31:197-208.
 48. Dissmeyer N, Rivas S, Graciet E. Life and death of proteins after protease cleavage: protein degradation by the N-end rule pathway. *New Phytol* 2018;218:929-35.

49. Joachimiak E, Waclawek E, Niziolek M, Osinka A, Fabczak H, Gaertig J, et al. The LisH domain-containing N-terminal fragment is important for the localization, dimerization, and stability of Katnal2 in Tetrahymena. *Cells* 2020;9:1-19.
50. Gerlitz G, Darhin E, Giorgio G, Franco B, Reiner O. Novel functional features of the Lis-H domain: role in protein dimerization, half-life and cellular localization. *Cell Cycle* 2005;4:1632-40.
51. Christidi E, Brunham LR. Regulated cell death pathways in doxorubicin-induced cardiotoxicity. *Cell Death Dis* 2021;12:339:1-15.
52. Szwed M, Kania KD, Jozwiak Z. Toxicity of doxorubicin-transferrin conjugate is connected to the modulation of Wnt/ β -catenin pathway in human leukemia cells. *Leuk Res* 2015;39:1096-102.
53. Xiao Q, Werner J, Venkatachalam N, Boonekamp KE, Ebert MP, Zhan T. Cross-talk between p53 and Wnt signaling in cancer. *Biomolecules* 2022;12:1-21.
54. Sadot E, Geiger B, Oren M, Ben-Ze'ev A. Down-regulation of β -catenin by activated p53. *Mol Cell Biol* 2001;21:6768-81.
55. Kim NH, Kim HS, Kim NG, Lee I, Choi HS, Li XY, et al. p53 and microRNA-34 are suppressors of canonical Wnt signaling. *Sci Signal* 2011;4:1-29.
56. Wellenstein MD, Coffelt SB, Duits DEM, van Miltenburg MH, Slagter M, de Rink I, et al. Loss of p53 triggers WNT-dependent systemic inflammation to drive breast cancer metastasis. *Nature* 2019;572:538-42.
57. Fischer U, Janicke RU, Schulze-Osthoff K. Many cuts to ruin: a comprehensive update of caspase substrates. *Cell Death Differ* 2003;10:76-100.
58. Faleiro L, Lazebnik Y. Caspases disrupt the nuclear-cytoplasmic barrier. *J Cell Biol* 2000;151:951-9.

59. Zhao L, Zhao J, Zhong K, Tong A, Jia D. Targeted protein degradation: mechanisms, strategies and application. *Signal Transduct Target Ther* 2022;7:1-13.
60. MacDonald BT, Tamai K, He X. Wnt/ β -catenin signaling: components, mechanisms, and diseases. *Dev Cell* 2009;17:9-26.
61. Dipalo M, Rastogi SK, Matino L, Garg R, Bliley J, Iachetta G, et al. Intracellular action potential recordings from cardiomyocytes by ultrafast pulsed laser irradiation of fuzzy graphene microelectrodes. *Sci Adv* 2021;7:1-9.
62. Clements M, Millar V, Williams AS, Kalinka S. Bridging functional and structural cardiotoxicity assays using human embryonic stem cell-derived cardiomyocytes for a more comprehensive risk assessment. *Toxicol Sci* 2015;148:241-60.
63. Shinlapawittayatorn K, Chattipakorn SC, Chattipakorn N. The effects of doxorubicin on cardiac calcium homeostasis and contractile function. *J Cardiol* 2022;80:125-32.
64. Kim SY, Kim SJ, Kim BJ, Rah SY, Chung SM, Im MJ, et al. Doxorubicin-induced reactive oxygen species generation and intracellular Ca^{2+} increase are reciprocally modulated in rat cardiomyocytes. *Exp Mol Med* 2006;38:535-45.
65. Kourek C, Touloupaki M, Rempakos A, Loritis K, Tsoungkos E, Paraskevaidis I, et al. Cardioprotective strategies from cardiotoxicity in cancer patients: A comprehensive review. *J Cardiovasc Dev Dis* 2022;9:1-15.

ABSTRACT (IN KOREAN)

TBL1X 단백질 절단 억제를 통한 독소루비신 유도 심근독성의 완화

<지도교수 윤 호 근>

연세대학교 대학원 의과학과

이 선 호

독소루비신(Doxorubicin)은 항암치료에 널리 사용되는 안트라사이클린 (anthracycline) 계열의 약물로, 독소루비신 유발 심근독성(Doxorubicin-induced cardiotoxicity; DICT)이라는 부작용을 가진다. 독소루비신 유발 심근독성의 병태생리학은 아직 완전히 밝혀지지 않았으며, 예방 또는 치료를 위한 효과적인 전략도 아직 개발되지 않았다. 본 연구에서는 독소루비신 유발 심근독성에 있어서 Transducin beta like 1-linked (TBL1X)의 새로운 역할을 규명하였다. TBL1X는 심장에서 높게 발현되며, nuclear factor kappa-light-chain-enhancer of activated B cells (NF- κ B), 유전자 전사 조절 및 WNT 신호전달 경로에서의 역할이 연구되어 왔다.

본 연구에서는 확장성 심근병증(Dilated cardiomyopathy; DCM) 환자에서 TBL1X 단백질의 발현이 낮음을 확인하였으며, 이는 TBL1X의 단백질 절단에 의한 것임을 밝혔다. 먼저, 쥐(rat) 심근세포주 H9c2에 독소루비신을 처리 시

caspase-3가 활성화되었으며, 이는 TBL1X의 125, 136, 215번째 아스파르트산 (Aspartate; D) 부위를 인지하여 절단시켰다. 단백질 절단과 관련된 기전 연구를 위해 세 부위의 아스파르트산을 알라닌 (Alanine; A)으로 모두 치환하여 절단이 일어나지 않는 변이체인 un-cleavable TBL1X(TBL1X^{uclv})를 제작하였다. 정상형 TBL1X와 다르게 절단된 TBL1X는 유비퀴틴 (Ubiquitin) 의존적 분해를 통해 불안정화되어 β -catenin과의 결합이 감소되었고 Axin2 및 Ccnd1 유전자의 프로모터 (promoter) 지역을 점유하지 못하여 WNT 신호전달 활성화가 감소되었다. 또한, 독소루비신에 의한 세포사멸사도 TBL1X^{uclv} 과발현 시 완화되었다.

동일한 결과가 사람 줄기세포 및 동물모델에서도 나타나는지 확인하기 위해 추가 연구를 진행하였다. 그 결과, 정상형 사람유도만능줄기세포 유래 심근세포(human induced pluripotent stem cell-derived cardiomyocytes; hiPSC-CMs)에 TBL1X^{uclv}를 과발현하면 세포사멸사가 완화되고 독소루비신에 의해 나타나는 박동 능력 감소, 전도율 지연 및 불규칙성 등의 전기생리학적 특성이 개선되는 것을 확인하였다. 마지막으로, 생쥐 (mouse) 심장 조직에서도 아데노연관바이러스 (Adeno-associated virus; AAV)를 이용하여 심장 특이적으로 과발현 시 정상형 대비 TBL1X^{uclv}에서 독소루비신에 의한 심근수축기능 저해와 콜라겐 축적을 개선시켜 심근독성을 감소시켰다.

결론적으로, 이러한 결과들은 독소루비신을 통해 TBL1X 단백질이 caspase-

3에 의존적으로 절단되고 이로 인해 WNT 신호전달이 억제되어 심근세포의 세포사멸사가 유도된다는 점을 시사한다. 또한, TBL1X 단백질의 새로운 역할을 규명하였고 환자의 암 치료 중 발생하는 독소루비신 유도 심근독성을 완화시킬 수 있어 효과적인 치료 전략을 구체화하는데 용이하게 할 것이다.

핵심되는 말 : TBL1X, 확장성 심근병증, 독소루비신, 사람유도만능줄기세포유래심근세포, WNT

PUBLICATION LIST

1. Oh J, **Lee SH**, Choi J, Choi JR, Kim S, Cha YJ, et al. Establishment of a novel human iPSC line (YCMi003-A) from a patient with dilated cardiomyopathy carrying genetic variant LMNA p.Asp364His. *Stem Cell Tes* 2021;56:102508-13. (*Published*)
2. **Lee SH**, Oh J, Lee ST, Won D, Kim S, Choi HK, et al. Generation of a human induced pluripotent stem cell line YCMi004-A from a patient with dilated cardiomyopathy carrying a protein-truncating mutation of the Titin gene and its differentiation towards cardiomyocytes. *Stem Cell Res* 2022;59:102629-34. (*Published*)
3. Jeong Y, **Lee SH**, Lee J, Kim MS, Lee YG, Hwang JT, et al. Water extract of *Capsella bursa-pastoris* mitigates doxorubicin-induced cardiotoxicity by upregulating antioxidant enzymes. *Int J Mol Sci* 2023;24:15912-15930. (*Published*)
4. **Lee SH**, Lee JH, Oh J, Hwang JT, Lee HJ, Byun HK, et al. Inhibition of TBL1 cleavage alleviates doxorubicin-induced cardiomyocytes death by regulating the Wnt/ β -catenin signal pathway. *Cardiovasc Res* 2024;00:00-00. (*Revision in progress*)